CHAPTER 4

Design, Synthesis and Biological Evaluation of *S*-Acetohydrazones of 1,3,4-Thiadiazole-2-Thiol

4. *S*-Acetohydrazones of 1,3,4-thiadiazole-2-thiol (TEH Series)

4.1. Design rationale and plan of work

4.1.1. Design rationale

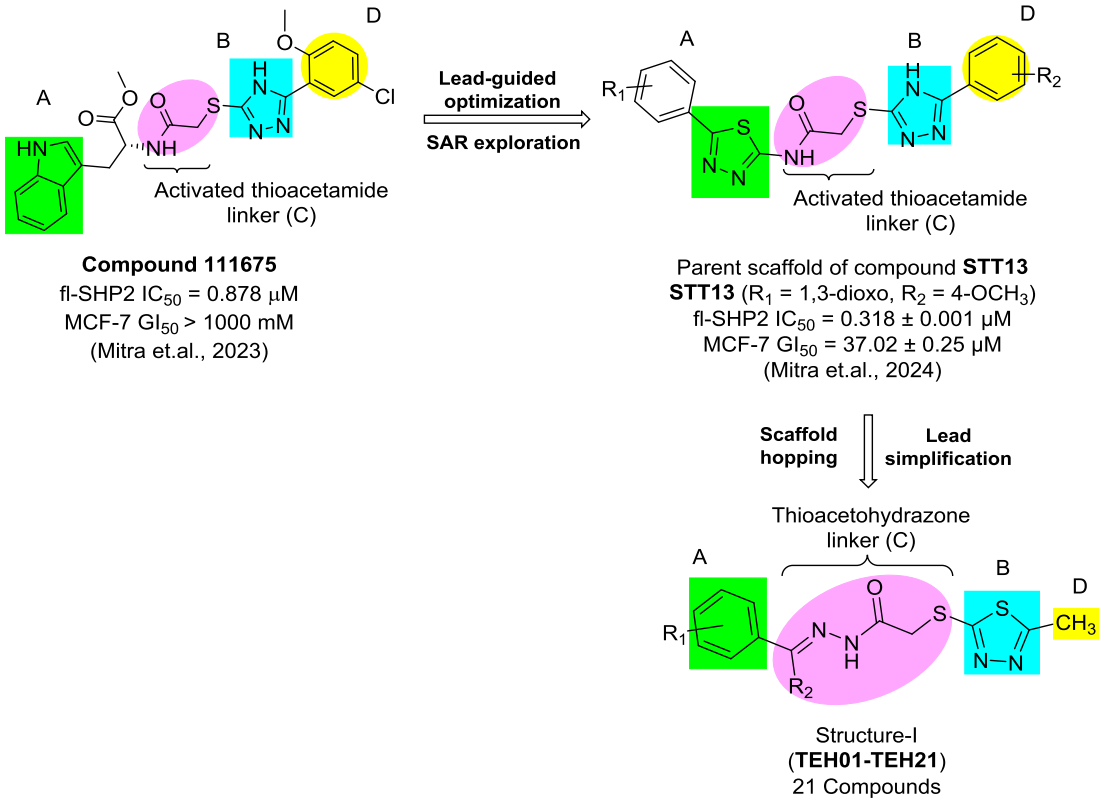

Figure 4.1. Design rationale of compounds **TEH01-TEH21**

Akin to compound **STT13** (SHP2 IC_{50} = 0.318 ± 0.001 µM, MCF-7 GI_{50} = 37.02 ± 0.25 µM) (**Figure 4.1**) previously developed [110, 173] through lead-guided optimization of compound **111675,** the current series consisting of structure-I (**Figure 4.1**) was designed using similar design strategies from the parent scaffold of compound **STT13** by simplifying the structure to improve upon the potency against SHP2. Lead

simplification was envisaged as a means to improve SHP2 binding and the resultant inhibitory potential after analysing the *in silico* binding pattern of compound **STT13** and its parent scaffold [173].

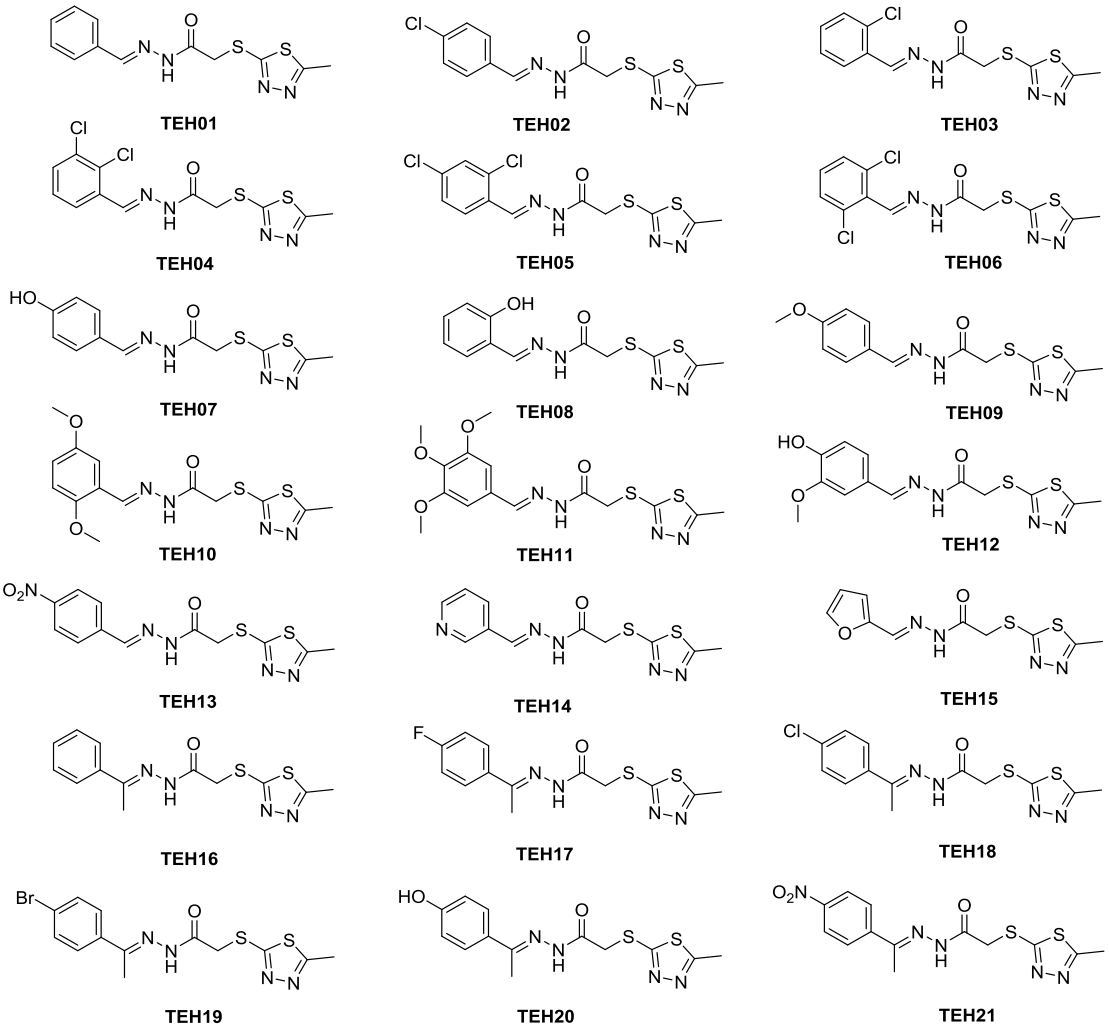

Figure 4.2. Skeletal formulae of rationally designed compounds (**TEH01**-**TEH21**)

The simplification was done by i) replacing the 1,3,4-thiadiazole moiety from part A of the heterocyclic hybrid with a linear imine group (-C=N-) thereby retaining only the substituted aryl ring (site A) and thus extending the thioacetamide linker (C, **Figure 4.1**) to the more functionalized and bioactive thioacetohydrazone linker (which is analogous to an *N*-acyl hydrazone moiety), ii) replacing the 1,2,4-triazole ring (B, **Figure 4.1**) with the bioisosteric 1,3,4-thiadiazole ring (site B) and iii) replacing the

substituted aryl ring (D, **Figure 4.1**) with the less steric methyl group thereby decreasing the lipophilicity of centre D. Inherently, acetohydrazones are recognized as privileged scaffolds in drug development for their favourable physicochemical properties and a wide range of potent biological activities including antiproliferative and anticancer activities [174-176]. This is due to the fact that they are quite easy to synthesize and can be widely functionalized and derivatized to give distinct compounds having diverse pharmacological profiles [177]. A set of 21 molecules was designed and synthesized and evaluated (**Figure 4.2**).

4.1.2. Plan of work

The plan of work for the design and development of the current series of compounds (**STS01-STS25**) is represented schematically in **Figure 4.3**. Lead-guided optimization via structural simplification was applied to design and synthesize a set of new analogous molecules which were subsequently evaluated biologically by *in vitro, in cellulo, in vivo* and *ex vivo* studies for desired efficacy and undesired toxicity.

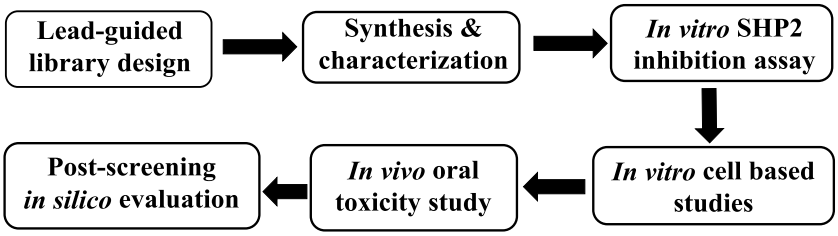

Figure 4.3. Schematic workflow for plan of work

4.2. Experimental work

4.2.1. Chemistry

4.2.1.1. Synthesis of compounds TEH01-TEH21

Laboratory grade synthetic reagents were procured from Sigma-Aldrich Chemical Private Ltd., India, Merck India, Fischer Scientific Ltd., Central Drug House (P) Ltd.

India, Loba Chemie India, Sisco Research Laboratories Pvt Ltd., India etc. and used as such without further purification. In general, reaction was monitored by TLC with the help of pre-coated silica gel plates (Merck, Kieselgel 60F-254, 0.20 mm).

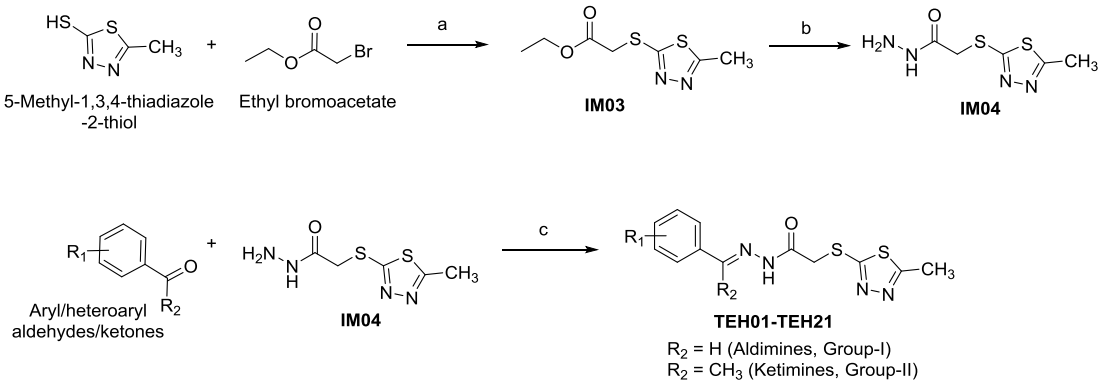

Scheme 4.1. Synthesis of compounds **TEH01-TEH21**. *Reagents & conditions*: (a) K_2CO_3, acetone, 0-5 ºC to RT, 1-2 h, 94% yield; (b) hydrazine hydrate, ethanol, reflux, 4-5 h, 97% yield; (c) glacial acetic acid, ethanol, RT to reflux, 2-3 h, 67-97% yield.

Step 1: Synthesis of intermediate IM03

To a solution of 5-methyl-1,3,4-thiadiazole-2-thiol (15.13 mmol) in dry acetone (40 mL) was added at RT powdered potassium carbonate (30.26 mmol) and cooled to 0-5°C. Ethyl bromoacetate (30.26 mmol) was added slowly to the reaction mixture and stirred at 0-5°C for 10 min after which the reaction was allowed to warm to ambient temperature and stirred for another 1-2 h. Progress of reaction was monitored by TLC. Once the reaction was complete, acetone was evaporated under reduced pressure, and to the residue was added water (100 mL) and extracted with ethyl acetate (2×50 mL). After washing the organic layer with brine (2×50 mL) and drying over anh. Na_2SO_4 the organic layer was evaporated in a rotavapor to obtain the intermediate **IM03** as a viscous oil (crude yield = 98%) which solidified on cooling and storing overnight. The crude product was purified by column chromatography to give the desired product in 93% yield.

Step 2: Synthesis of intermediate IM04

To a stirred solution of ethyl 2-((5-methyl-1,3,4-thiadiazol-2-yl)thio)acetate **(IM03)** (6.88 mmol) in absolute ethanol (25 mL), was added hydrazine hydrate (34.4 mmol) dropwise at RT. The reaction mixture was heated to reflux and stirred for 3-4 h and then at RT overnight after which white precipitate was seen in the reaction. Progress of the reaction was monitored by TLC. Upon completion of reaction, the white precipitate was filtered under reduced pressure, washed with cold ethanol (10 mL) and sucked dry. The product was unloaded and dried in a vacuum tray drier at 60-70°C to give desired intermediate **IM04** as a white solid (83% yield).

Step 3: General procedure for the synthesis of compounds TEH01-TEH21

The final compounds **TEH01-TEH21** were synthesized by the reaction of different substituted benzaldehydes or acetophenone derivatives with 2-((5-methyl-1,3,4-thiadiazol-2-yl)thio)acetohydrazide (**IM04**) in the presence of catalytic amount of glacial acetic acid at RT to reflux. Each of the starting material and intermediate **IM04** were dissolved in 1:1 stoichiometric ratio in absolute ethanol (20-25 mL) and a few drops of glacial acetic acid was added and stirred at RT or refluxed for 2-3 h. Progress and completion of reaction was monitored by TLC. On completion, the reaction mass was cooled to 0-5°C and the resultant white precipitate was filtered under reduced pressure, washed with ethanol and sucked dry. Recrystallization from absolute ethanol gave the desired final compounds **TEH01-TEH21** as powdery solids.

4.2.1.2. Physicochemical characterization

The physicochemical characterizations of all the synthesized compounds of the **TEH series** were performed for melting range, solubility, retardation factor (R_f), calculated

logP (ClogP), experimental logP (i.e., partitioning in *n*-octanol:water) and appearance of the final compounds (**TEH01-TEH21**) by identical methodologies as described in Chapter 2 (**Section 2.2.2.3**).

4.2.1.3. Spectral characterization

The spectral characterization of the intermediates and final compounds (**TEH01-TEH21**) was done to elucidate their structure and confirm their formation by ATR-FTIR, ^{1}H & ^{13}C NMR, MS and HRMS techniques as described in **Section 2.2.2.4**. The ATR-FTIR spectroscopy of the final compounds was carried out using a Jasco FT/lR-6X FTIR spectrometer where a few crystals/particles of each compound was placed on the dedicated platform and the ATR measurements recorded by the instrument.

4.2.2. Biological studies

4.2.2.1. *In vitro* SHP2 enzyme inhibition assay

The biochemical *in vitro* assay to evaluate SHP2 inhibition activity of the compounds **TEH01-TEH21** was done by following the fluorescence-based DiFMUP assay using the homogeneous full-length SHP-2 assay kit by allosterically activating fl-SHP2 enzyme prior to substrate addition by incubating with IRS-1 peptide (mentioned in **Section 2.2.3.1**). All experiments were done in duplicate using three different concentrations of the test compounds and results are reported as mean ± SEM.

4.2.2.2. Cell-based assays

4.2.2.2.1. *In vitro* antiproliferation study in cancer cell lines

The *in vitro* antiproliferation efficacy of compounds **TEH01-TEH21** was assessed by an MTT assay on MCF-7 cells as described earlier in **Section 2.2.3.4.2**. All experiments were done in triplicate and results are reported as mean ± SEM.

4.2.2.2.2. Colony formation assay and scratch wound-healing assay of compounds TEH06 and TEH19

The anti-survival and anti-migratory property of compounds **TEH06** and **TEH19** in MCF-7 cells was determined by conducting a colony formation and scratch wound-healing assay respectively. The protocol for the assay has been described previously in **Section 2.2.3.4.3** and was followed without any modifications for the current assay.

4.2.2.3. *In vivo* studies

4.2.2.3.1. *In vivo* acute oral toxicity evaluation of compound TEH06

All animal experimentations conducted were approved by the Institutional Animals Ethics Committee (IAEC) of Indian Institute of Technology (Banaras Hindu University), Varanasi, India (IAEC Approval Number: IIT(BHU)/IAEC/2024/I/039). The acute oral toxicity of compound **TEH06** was determined in adult female albino mice in accordance with the OECD Guideline 423 (Acute Toxic Class Method) and the LD_{50} calculated. The method followed for the study and the parameters tested are mentioned in **Section 2.2.3.5.1**.

4.2.3. Computational studies

Post-screening molecular docking of compound **TEH01-TEH21** was done in the tunnel allosteric site of SHP2 (PDB ID: 5EHR) to assess their binding affinity and pose analysis in SHP2 allosteric site. This was done in AutoDockTools 4.2 by using the protocol as described earlier in **Section 2.2.4.1** and visualizing the docked conformations in Discovery Studio Visualizer v21.1.0.20298. Further, molecular dynamics simulation study was done for compound **TEH06** for 100 ns in the tunnel allosteric site of SHP2 (PDB ID: 5EHR) using Desmond module (described in **Section**

2.2.4.2). Finally, the ADMET properties of the molecules of the **STS series** were predicted using Pre-ADMET web-based server (**Section 2.2.4.3**).

The BOILED-egg model was used to generate ADME-related calculation for our compounds **TEH01-TEH21** and the clinical SHP2 inhibitors. The BOILED-egg is an 'intuitive graphical classification model for gastrointestinal absorption and brain access' developed by Molecular Modelling Group of Swiss Institute of Bioinformatics and University of Lausanne. The model was accessed through their web server http://www.swissadme.ch/, on 12th May 2024. The test compounds were imported to the appropriate module of the SwissADME server as the corresponding SMILES notations which were generated by ChemDraw Professional 15.0.0.106. Upon running the calculations in the server, the BOILED-egg model for the molecules was generated and reported.

Few important PK and bioavailability parameters of our lead compound **TEH06** were predicted using Deep-PK, a robust machine learning method based on diverse molecular descriptors and graph neural networks developed by the Biosig Lab at The University of Queensland, and accessible through the following web server, https://biosig.lab.uq.edu.au/deeppk/prediction, accessed on 10th June, 2024. The structure of **TEH06** was imported into the predictor module in the form of the corresponding SMILES string generated by ChemDraw Professional 15.0.0.106, followed by the predictive calculations which were generated and reported. Some of the parameters were further calculated from the above predicted data using the Pharmacokinetic Simulator accessible via the following web-based server, http://www.vulpinescience.co.uk/uploads/MedChem%20Calculators_Ver3.2/MedChem%20Calculators.htm (accessed on 10th June, 2024), developed by Dr. David Fox of the Vulpine Science and Learning Limited, West Stourmouth, England, UK.

4.3. Results and discussion

4.3.1. Chemistry

4.3.1.1. Synthesis of final compounds TEH01-TEH21

The final compounds of the current series i.e., **TEH01** to **TEH21** were synthesized using conventional methodology wherein the key starting material 5-methyl-1,3,4-thiadiazole-2-thiol was converted to the corresponding thioether (**IM03**) using ethyl 2-bromoacetate in a base catalysed condition, followed by its hydrazinolysis to give the corresponding hydrazide derivative (**IM04**) in quantitative yield. This hydrazide was utilized to prepare a number of suitable carbohydrazones (**TEH01-TEH21**) by condensing them with appropriate aryl carbonyls like substituted benzaldehydes (Group-I) and substituted acetophenones (Group-II) to give the final compounds in good yield (**Scheme 4.1**).

4.3.1.2. Physicochemical characterization of final compounds

All the final compounds of **TEH** series (**TEH01-TEH21**) were obtained in good yield ranging from 67-97 % as powdered solid. Physicochemical characteristics of the final compounds like melting point, ClogP and experimental logP (*n*-octanol/water) of the lead compound i.e., **TEH06** were determined and are given in **Table 4.1**. Compound **TEH06** possessed a logP of 1.12 in n-octanol:water indicating a less lipophilic molecule.

Table 4.1. Physicochemical characterization data of compounds **TEH01-TEH21**.

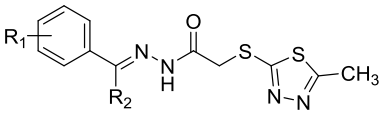

TEH01-TEH13, TEH16-TEH21

R_2 = H (Aldimines, Group-I)
R_2 = CH_3 (Ketimines, Group-II)

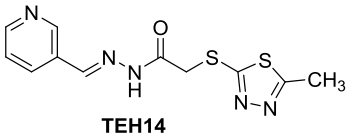

TEH14

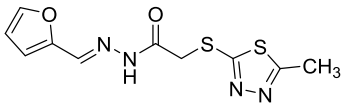

TEH15

Compd Code	R_1	R_2	MW	ClogP[a]	% yield	Melting range (°C)	R_f[b]	Appearance
TEH01	H	H	292.38	1.277	99	115-117	0.77	White solid
TEH02	4-Cl	H	326.82	1.99	85	152-154	0.68	White solid
TEH03	2-Cl	H	326.82	2.14	86	132-133	0.85	White solid
TEH04	2,3-Cl_2	H	361.26	1.983	96	138-140	0.74	White solid
TEH05	2,4-Cl_2	H	361.26	2.103	91	158-160	0.75	White solid
TEH06	2,6-Cl_2	H	361.26	1.503	85	150-152	0.80	White solid
TEH07	4-OH	H	308.37	1.246	96	168-170	0.66	White solid
TEH08	2-OH	H	308.37	1.875	89	174-176	0.58	White solid
TEH09	4-OMe	H	322.40	1.496	81	96-97	0.72	White solid
TEH10	2,5-di-OMe	H	338.40	1.135	98	159-160	0.75	White solid
TEH11	3,4,5-tri-OMe	H	382.45	0.676	85	168-169	0.90	White solid
TEH12	3-OMe-4-OH	H	352.43	0.888	87	142-144	0.60	White solid
TEH13	4-NO_2	H	337.37	1.02	97	163-165	0.66	White solid
TEH14	-	-	293.36	-0.04	98	153-155	0.85	White solid
TEH15	-	-	282.34	0.453	83	148-150	0.73	White solid
TEH16	H	CH_3	306.40	2.613	93	96-98	0.80	White solid
TEH17	4-F	CH_3	324.39	2.756	85	142-144	0.82	White solid
TEH18	4-Cl	CH_3	340.84	3.326	78	156-158	0.85	White solid
TEH19	4-Br	CH_3	385.30	3.476	88	146-148	0.90	White solid
TEH20	4-OH	CH_3	322.40	1.946	54	156-158	0.55	White solid
TEH21	4-NO_2	CH_3	351.40	2.356	81	195-197	0.76	White solid

[a] Calculated using ChemDraw v15.0.0.106; [b] R_f values are in 60% EtOAc-Hexane

4.3.1.3. Spectral characterization

The compounds were characterized by FTIR, ^{1}H & ^{13}C NMR and HRMS analysis. The spectral data of the key intermediates of this series i.e., **IM03** and **IM04** are given below. The compounds were confirmed by ^{1}H NMR by the appearance of signals at δ 4.23 ppm, δ 4.12 ppm and δ 1.29 ppm corresponding to the thioacetate methylene

protons [-S-C**H**$_2$-CO-], the methoxy methylene protons [-CO-C**H**$_2$-CH$_3$] and the methyl protons of the methoxy group [-CO-CH$_2$-C**H**$_3$]. The hydrazinolysis of **IM03** to form **IM04** was confirmed by disappearance of peaks at δ 4.23 and δ 4.12 and appearance of two distinct peaks at δ 3.95 (1 proton) and δ 3.96 ppm (2 protons) corresponding to the hydrazide protons [-CO-N**H**-N**H**$_2$], respectively.

Ethyl 2-((5-methyl-1,3,4-thiadiazol-2-yl)thio)acetate (IM03): ^{1}H NMR (500 MHz, $CDCl_3$) δ ppm 4.23 (q, *J* = 7.1 Hz, 2H), 4.12 (s, 2H), 2.73 (s, 3H), 1.29 (t, *J* = 7.2 Hz, 3H); ^{13}C NMR (126 MHz, $CDCl_3$) δ ppm 167.98, 165.56, 163.57, 62.16, 35.47, 15.65, 14.09.

2-((5-Methyl-1,3,4-thiadiazol-2-yl)thio)acetohydrazide (IM04): m.p.: 117-118°C; ^{1}H NMR (500 MHz, $CDCl_3$) δ ppm 8.42 (s, 1H), 3.96 (s, 2H), 3.95 (s, 1H), 2.76 (s, 3H); ^{13}C NMR (126 MHz, $CDCl_3$) δ ppm 168.60, 165.79, 165.18, 34.31, 15.70.

The formation of the final compounds was primarily proved by FTIR/FTATR spectroscopy wherein the appearance of amide C=O and imine C=N str. vibrations at ν 1654–1700 cm^{-1} and ν 1556–1599 cm^{-1}, and NH absorption band around ν 3177–3230 cm^{-1}, confirmed the *S*-acyl hydrazone backbone in all the compounds.

Interestingly, the NMR analytical data of all the compounds indicated the presence of rotational isomers or rotamers (*synperiplanar* or *antiperiplanar,* **Figure 4.4**) in varying ratio of *syn* to *anti* isomer. This isomerism in acyl hydrazone derivatives has been previously reported [178] where the major stereochemical factor was ascertained to be restricted rotation about the C-N bond of the amide linkage, C(O)-NH. However, geometrical isomers i.e., *Z* and *E* isomers arising due to rotation along the imine C=N bond which are a theoretical possibility are not favored in our case due to steric

overcrowding (vide **Figure 4.4**) and also due to removal of intramolecular hydrogen bonding of the *Z*-isomer (**Figure 4.4**) in polar solvent like DMSO-d_6[179, 180]. In the current scenario, we did not observe the *Z*-isomer in any molecule of our library even in less polar solvent like $CDCl_3$ indicating an overarching steric effect coming into play which means only the *E*-isomer is the preferred outcome. To further corroborate the above interpretation, it can be pointed out that while the NH proton of *Z*-isomers of acyl hydrazones are reported to have chemical shifts around δ 14 ppm [181], no compounds of this series displayed any signal in that region (see **Figure 4.5** for a representative PMR spectra of compound **TEH06**). Finally, the presence of *Z*-isomer of compounds **TEH01**-**TEH21** was unequivocally ruled out by conducting thin-layer chromatography of each final compound wherein only a single spot was obtained in each case [182].

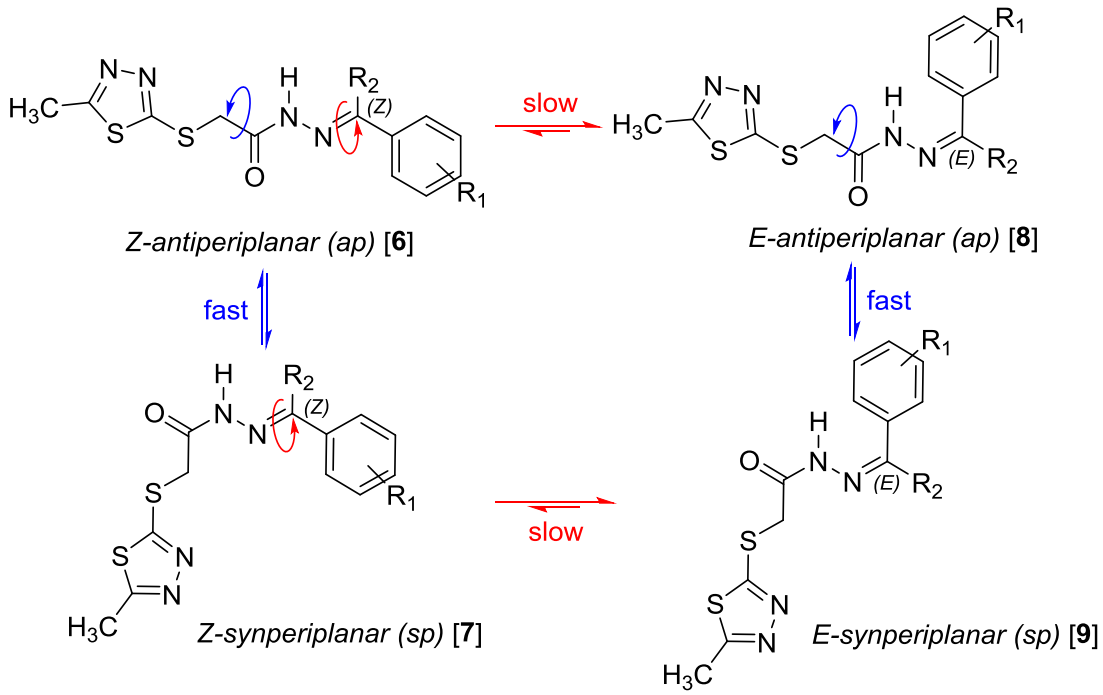

Figure 4.4. Possible rotational isomers in synthesized compounds of the current series arising due to C-N bond -CO-NH rotation.

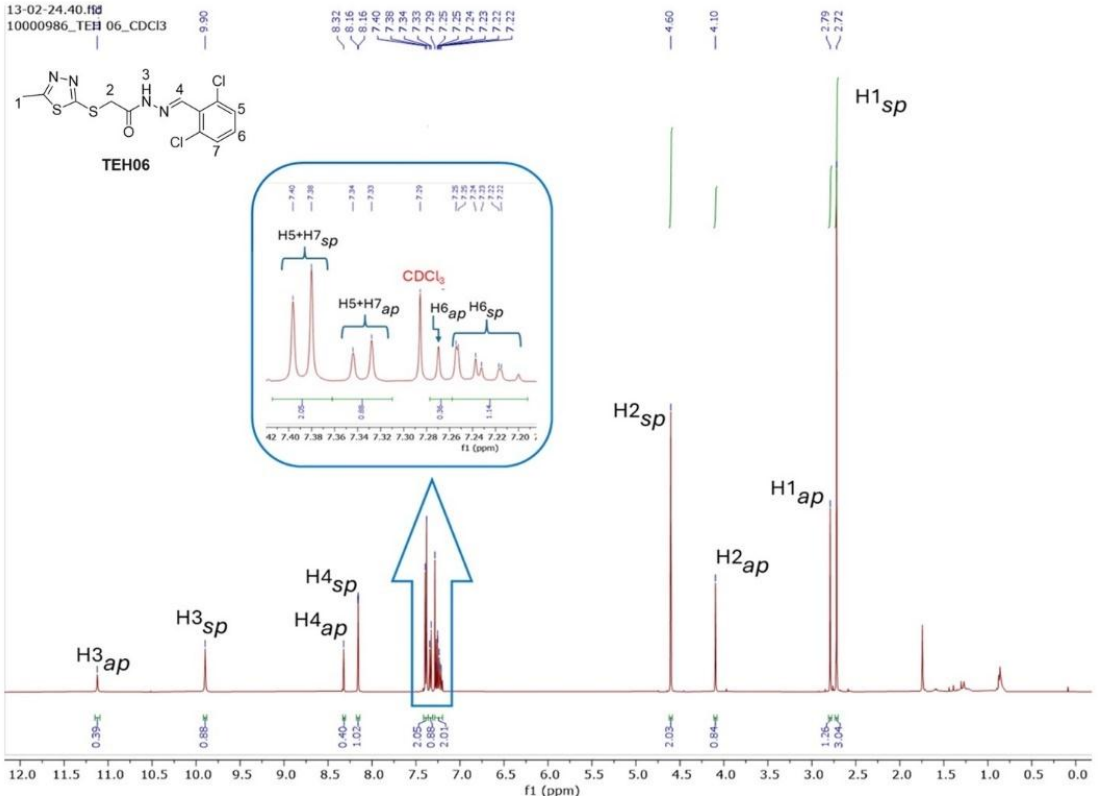

Figure 4.5. Representative 500 MHz ^{1}H NMR spectra of compound **TEH06** in $CDCl_3$ depicting the *synperiplanar* (*sp*) and *antiperiplanar* (*ap*) signals (peaks). The H-suffix denotes the same protons as shown in the structure of compound **TEH06** in inset of the figure.

Table 4.2 tabulates all the duplicated signals/peaks obtained in ^{1}H NMR spectroscopy for compounds **TEH01-TEH21**. Distinct pairs of signals were observed for the amide -C(O)-NH, imine -N=CH, methylene -CH_2-CO protons, along with for the thiadiazole 5-methyl protons. All other specific sets of protons of individual functional groups of the various analogs also displayed signal duplicity in the same ratio as the above four types of protons. This rotamer ratio apparently was not dependent on the NMR solvent used and was solely due to the electronegative and steric effect of such substituents which resulted in dissimilar ratio of *syn* vs. *anti* isomers from one analog to the other. For example, no substitution in the aryl ring or smaller substituents at the *para*-position resulted in 50:50 mixture of both *syn* and *anti*-isomers due to less steric crowding and

facilitated stereochemical switch between the two isomers at ambient temperature. For the same reason, with bigger groups or multiple substitutions at the aryl ring, the ratio was skewed in favor of the *syn*-isomer. Similarly, for the acetophenone derivatives i.e., compounds of Group-II, all molecules displayed more *syn*-isomers due to presence of the additional methyl group at the imine carbon making it more restrictive towards stereoisomeric switch. No further attempts were made to separate the rotamers and were taken as such for the *in vitro* assays and subsequent evaluations.

Table 4.2. Chemical shifts of duplicated signals in ^{1}H NMR of compounds **TEH01-TEH21**

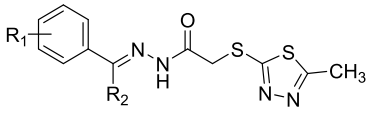

TEH01-TEH13, TEH16-TEH21

R_2 = H (Aldimines, Group-I)
R_2 = CH_3 (Ketimines, Group-II)

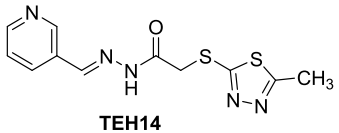

TEH14

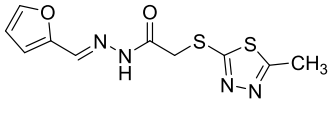

TEH15

Compound Details				Chemical Shift δ (ppm)									
Compd Code	**R_1**	**R_2**	**Solvent**	C(O)-N**H**		N=C**H** / N=C(C**H**$_3$)		C**H**$_2$-CO		TDZ-C**H**$_3$		Ar-**H** Range	Ratio (*syn*:*anti*)
				syn-	*anti*-	*syn*-	*anti*-	*syn*-	*anti*-	*syn*-	*anti*-		
TEH01	H	H	$CDCl_3$	9.49	10.91	7.84	8.09	4.67	4.05	2.72	2.80	7.36-7.77	1:1
TEH02	4-Cl	H	$CDCl_3$	10.11	11.02	7.86	8.06	4.66	4.05	2.71	2.79	7.32-7.71	1:1
TEH03	2-Cl	H	$CDCl_3$	9.94	11.01	8.32	8.52	4.67	4.10	2.72	2.78	7.24-8.14	1:0.75
TEH04	2,3-Cl_2	H	$CDCl_3$	9.70	11.09	8.31	8.54	4.67	4.08	2.73	2.80	7.20-8.54	1:1
TEH05	2,4-Cl_2	H	DMSO-d_6	11.94	12.08	8.36	8.55	4.61	4.18	2.67	2.69	7.52-7.97	1:0.5
TEH06	2,6-Cl_2	H	$CDCl_3$	9.90	11.12	8.16	8.32	4.60	4.10	2.72	2.79	7.22-7.39	1:0.4
TEH07	4-OH	H	DMSO-d_6	11.53	11.59	7.92	8.09	4.55	4.14	2.67	2.68	6.82-7.92	1:0.5
TEH08	2-OH	H	DMSO-d_6	10.97	10.08	8.43	8.34	4.57	4.19	2.67	2.68	6.86-7.69	1:1
TEH09	4-OMe	H	$CDCl_3$	10.05	10.82	7.83	8.02	4.64	4.05	2.70	2.77	6.86-7.72	1:0.8
TEH10	2,5-di-OMe	H	$CDCl_3$	10.74	--[a]	8.24	8.46	4.62	4.07	2.70	2.77	6.81-7.54	1:0.75
TEH11	3,4,5-tri-OMe	H	$CDCl_3$	10.96	10.00	8.02	7.80	4.65	4.04	2.70	2.79	6.91-6.97	1:0.75
TEH12	3-OMe-4-OH	H	DMSO-d_6	11.56	11.61	7.91	8.08	4.56	4.14	2.66	2.68	6.83-7.27	1:0.6

TEH13	4-NO_2	H	DMSO-d_6	12.01	12.09	8.14	--[b]	4.63	4.21	2.67	2.69	7.92-8.33	1:0.5
TEH14	-	-	DMSO-d_6	11.88	11.95	8.07	8.27	4.61	4.19	2.67	2.69	7.44-8.88	1:0.5
TEH15	-	-	$CDCl_3$	10.93	10.01	8.08	7.78	4.61	4.04	2.78	2.72	6.49-7.52	1:0.75
TEH16	H	CH_3	$CDCl_3$	8.88	10.89	2.47	2.27	4.07	4.68	2.79	2.73	7.35-7.85	1:0.8
TEH17	4-F	CH_3	$CDCl_3$	9.09	10.91	2.35	2.25	4.06	4.67	2.79	2.73	7.02-7.86	1:0.7
TEH18	4-Cl	CH_3	$CDCl_3$	9.18	10.95	2.34	2.25	4.06	4.66	2.79	2.73	7.31-7.81	1:0.7
TEH19	4-Br	CH_3	$CDCl_3$	8.80	10.95	2.34	2.24	4.06	4.66	2.79	2.74	7.47-7.75	1:0.5
TEH20	4-OH	CH_3	DMSO-d_6	9.77	10.80	2.21	2.23	4.58	4.25	2.67	2.69	6.76-7.68	1:0.5
TEH21	4-NO_2	CH_3	$CDCl_3$	11.22	8.92	2.42	2.32	4.08	4.70	2.80	2.75	7.91-8.31	1:0.4

[a] Very weak or no signal detected; not integrable; [b] Signal overlapped with aromatic signals

(*E*)-*N*'-Benzylidene-2-((5-methyl-1,3,4-thiadiazol-2-yl)thio)acetohydrazide (**TEH01**): White solid; yield = 99%, m.p.: 115-117 ºC; FTIR (*v*, cm^{-1}, KBr) 3209 (amide N-H str.), 3075 (aromatic C-H str.), 1700 (amide C=O str.), 1562 (C=N str.), 1389 (aromatic amine C-N str.), 1233 (amine C-N str.); ^{1}H NMR (500 MHz, $CDCl_3$) δ ppm 10.91 (s, 1H), 9.49 (s, 1H), 8.09 (s, 1H), 7.84 (d, *J* = 0.8 Hz, 1H), 7.77 (dq, *J* = 7.3, 2.8 Hz, 2H), 7.72 – 7.65 (m, 2H), 7.47 – 7.36 (m, 6H), 4.67 (s, 2H), 4.05 (s, 2H), 2.80 (s, 3H), 2.72 (s, 3H); ^{13}C NMR (126 MHz, $CDCl_3$) δ ppm 169.14, 166.61, 166.14, 165.79 – 165.43 (m), 164.60, 164.33, 148.75, 144.88, 133.36, 133.19, 130.63, 128.85, 128.65, 127.89, 127.43, 36.03, 35.32, 15.82, 15.72, 15.62; HRMS: calcd for $C_{12}H_{12}N_4OS_2$ $[M+H]^+$ 293.0531, found. 293.0527.

(*E*)-*N*'-(4-Chlorobenzylidene)-2-((5-methyl-1,3,4-thiadiazol-2-yl)thio)acetohydrazide (TEH02): White solid; yield = 85%, m.p.: 152-154 ºC; ATR-FTIR (*v*, cm^{-1}, neat) 3219 (amide N-H str.), 3083 (aromatic C-H str.), 1687 (amide C=O str.), 1566 (C=N str.), 1323 (aromatic amine C-N str.), 1187 (amine C-N str.), 728 (C-Cl str.); ^{1}H NMR (500 MHz, $CDCl_3$) δ ppm 11.02 (s, 1H), 10.11 (s, 1H), 8.06 (s, 1H), 7.86 (s, 1H), 7.71 – 7.65 (m, 2H), 7.64 – 7.58 (m, 2H), 7.42 – 7.32 (m, 4H), 4.66 (s, 2H), 4.05 (s, 2H), 2.79 (s, 3H), 2.71 (s, 3H); ^{13}C NMR (126 MHz, $CDCl_3$) δ ppm 169.50, 166.62, 166.18, 165.64, 164.68, 164.29, 147.41, 147.35, 144.05, 143.98, 136.51, 136.41, 131.94, 131.84, 129.12, 129.00, 128.95, 128.58, 128.57, 35.87, 35.52, 35.39, 15.82, 15.72, 15.63; HRMS: calcd for $C_{12}H_{11}ClN_4OS_2$ $[M+H]^+$ 327.0141, found. 293.0137.

(*E*)-*N*'-(2-Chlorobenzylidene)-2-((5-methyl-1,3,4-thiadiazol-2-yl)thio)acetohydrazide (TEH03): White solid; yield = 86%, m.p.: 132-133 ºC; ATR-FTIR (*v*, cm^{-1}, neat) 3186 (amide N-H str.), 3083 (aromatic C-H str.), 1670 (amide C=O

str.), 1558 (C=N str.), 1365 (aromatic amine C-N str.), 1296 (amine C-N str.); 742 (C-Cl str.); ^{1}H NMR (500 MHz, $CDCl_3$) δ ppm 11.01 (s, 1H), 9.94 (s, 1H), 8.52 (s, 1H), 8.32 (s, 1H), 8.14 (dd, J = 7.7, 1.8 Hz, 1H), 7.98 (dd, J = 7.6, 2.0 Hz, 1H), 7.41 – 7.24 (m, 7H), 4.67 (s, 2H), 4.10 (s, 2H), 2.78 (s, 2H), 2.72 (s, 3H); ^{13}C NMR (126 MHz, DMSO-d_6) δ ppm 164.57, 161.48, 161.33, 160.91, 159.96, 159.60, 140.46, 140.31, 136.98, 136.90, 129.64, 129.63, 126.65, 126.23, 126.08, 125.27, 125.11, 123.34, 122.62, 122.55, 122.35, 31.35, 31.28, 31.21, 30.68, 11.03, 10.97, 10.93, 10.87; HRMS: calcd for $C_{12}H_{11}ClN_4OS_2$ $[M+H]^+$ 327.0141, found. 293.0131.

(*E*)-*N*'-(2,3-Dichlorobenzylidene)-2-((5-methyl-1,3,4-thiadiazol-2-yl)thio)acetohydrazide (TEH04): White solid; yield = 96%, m.p.: 138-140 ºC; ATR-FTIR (*ν*, cm^{-1}, neat) 3219 (amide N-H str.), 1670 (amide C=O str.), 1556 (C=N str.), 1360 (aromatic amine C-N str.), 1296 (amine C-N str.), 780 (C-Cl str.); ^{1}H NMR (500 MHz, $CDCl_3$) δ ppm 11.09 (s, 1H), 9.70 (s, 1H), 8.54 (s, 1H), 8.31 (s, 1H), 8.06 (dd, *J* = 8.0, 1.5 Hz, 1H), 7.91 (dd, *J* = 7.9, 1.5 Hz, 1H), 7.51 (ddd, *J* = 14.7, 7.9, 1.5 Hz, 2H), 7.28 – 7.20 (m, 2H), 4.67 (s, 2H), 4.08 (s, 2H), 2.80 (s, 3H), 2.73 (s, 3H); ^{13}C NMR (126 MHz, $CDCl_3$) δ ppm 169.11, 166.31, 166.14, 165.64, 164.81, 164.18, 144.81, 141.18, 133.69, 133.38, 133.24, 132.94, 132.48, 131.87, 131.83, 127.55, 127.41, 126.29, 125.52, 35.89, 35.40, 15.74, 15.64; HRMS: calcd for $C_{12}H_{10}Cl_2N_4OS_2$ $[M+H]^+$ 360.9751, found. 360.9745.

(*E*)-*N*'-(2,4-Dichlorobenzylidene)-2-((5-methyl-1,3,4-thiadiazol-2-yl)thio)acetohydrazide (TEH05): White solid; yield = 91%, m.p.: 158-160 ºC; ATR-FTIR (*ν*, cm^{-1}, neat) 3200 (amide N-H str.), 3058 (aromatic C-H str.), 1676 (amide C=O str.), 1564 (C=N str.), 866 (C-Cl str.), 820 (C-Cl str.); ^{1}H NMR (500 MHz, DMSO-d_6) δ ppm 12.08 (s, 1H), 11.94 (s, 1H), 8.55 (s, 1H), 8.36 (s, 1H), 7.97 (dd, *J* = 25.6, 8.6

Hz, 2H), 7.73 (t, *J* = 2.0 Hz, 2H), 7.52 (ddt, *J* = 8.6, 2.6, 1.3 Hz, 2H), 4.61 (s, 2H), 4.18 (s, 1H), 2.69 (s, 1H), 2.67 (s, 3H); ^{13}C NMR (126 MHz, DMSO-d_6) δ ppm 168.97, 166.11, 164.98, 139.43, 139.31, 135.53, 134.18, 130.77, 129.97, 129.79, 128.68, 128.49, 36.25, 15.75, 15.58; HRMS: calcd for $C_{12}H_{10}Cl_2N_4OS_2$ $[M+H]^+$ 360.9751, found. 360.9747.

(*E*)-*N*'-(2,6-Dichlorobenzylidene)-2-((5-methyl-1,3,4-thiadiazol-2-yl)thio)acetohydrazide (TEH06): White solid; yield = 85%, m.p.: 150-152 ºC; ATR-FTIR (*v*, cm^{-1}, neat) 3230 (amide N-H str.), 3041 (aromatic C-H str.), 1667 (amide C=O str.), 1583 (C=N str.), 1318 (aromatic amine C-N str.), 1272 (amine C-N str.), 775 (C-Cl str.); ^{1}H NMR (500 MHz, $CDCl_3$) δ ppm 11.12 (s, 1H), 9.90 (s, 1H), 8.32 (s, 0H), 8.16 (d, *J* = 1.1 Hz, 1H), 7.39 (d, *J* = 8.1 Hz, 2H), 7.34 (d, *J* = 8.1 Hz, 1H), 7.29 – 7.20 (m, 2H), 4.60 (s, 2H), 4.10 (s, 1H), 2.79 (s, 1H), 2.72 (s, 3H); ^{13}C NMR (126 MHz, $CDCl_3$) δ ppm 169.63, 166.44, 166.14, 165.62, 164.73, 164.30, 143.81, 139.85, 139.80, 135.26, 135.21, 130.44, 130.21, 129.17, 128.67, 35.92, 35.43, 15.82, 15.72, 15.62; HRMS: calcd for $C_{12}H_{10}Cl_2N_4OS_2$ $[M+H]^+$ 360.9751, found. 360.9751.

(*E*)-*N*'-(4-Hydroxybenzylidene)-2-((5-methyl-1,3,4-thiadiazol-2-yl)thio)acetohydrazide (TEH07): White solid; yield = 96%, m.p.: 168-170 ºC; ATR-FTIR (*v*, cm^{-1}, neat) 3082 (aromatic C-H str.), 1664 (amide C=O str.), 1582 (C=N str.), 1383 (aromatic amine C-N str.), 1280 (amine C-N str.), 1235 (phenolic C-O str.); ^{1}H NMR (500 MHz, DMSO-d_6) δ ppm 11.59 (s, 1H), 11.53 (s, 2H), 9.95 (s, 1H), 9.93 (s, 2H), 8.09 (s, 1H), 7.92 (s, 2H), 7.53 (d, *J* = 7.9 Hz, 4H), 7.51 (d, *J* = 2.0 Hz, 2H), 6.83 (d, *J* = 6.4 Hz, 4H), 6.82 (d, *J* = 1.0 Hz, 2H), 4.55 (s, 4H), 4.14 (s, 2H), 2.68 (s, 3H), 2.67 (s, 6H); ^{13}C NMR (126 MHz, DMSO-d_6) δ ppm 168.33, 166.22, 166.01, 165.28, 164.77, 163.12, 159.99, 159.82, 148.03, 147.87, 144.76, 144.59, 129.47, 129.35,

129.18, 129.08, 125.39, 116.25, 116.09, 36.66, 36.47, 15.74, 15.58; HRMS: calcd for $C_{12}H_{12}N_4O_2S_2$ $[M+H]^+$ 309.0480, found. 309.0475.

(*E*)-*N*'-(2-Hydroxybenzylidene)-2-((5-methyl-1,3,4-thiadiazol-2-yl)thio)acetohydrazide (TEH08): White solid; yield = 89%, m.p.: 174-176 ºC; ATR-FTIR (ν, cm^{-1}, neat) 3177 (amide N-H str.), 3011 (aromatic C-H str.), 1677 (amide C=O str.), 1568 (C=N str.), 1377 (aromatic amine C-N str.), 1273 (amine C-N str.), 1192 (phenolic C-O str.); ^{1}H NMR (500 MHz, DMSO-d_6) δ ppm 12.01 (s, 1H), 11.67 (s, 1H), 10.97 (s, 1H), 10.08 (s, 1H), 8.43 (s, 1H), 8.34 (s, 1H), 7.69 (dd, *J* = 7.8, 1.7 Hz, 1H), 7.56 (dd, *J* = 7.7, 1.7 Hz, 1H), 7.27 (dddd, *J* = 21.1, 8.2, 7.2, 1.7 Hz, 2H), 6.95 – 6.87 (m, 4H), 6.86 (dd, *J* = 7.5, 1.1 Hz, 1H), 4.57 (s, 2H), 4.19 (s, 2H), 2.68 (s, 3H), 2.67 (s, 3H); ^{13}C NMR (126 MHz, DMSO-d_6) δ ppm 168.38, 166.29, 166.01, 165.19, 164.62, 163.46, 157.75, 156.90, 147.78, 147.69, 141.84, 141.73, 132.02, 131.77, 129.54, 126.80, 126.64, 120.47, 119.92, 119.81, 119.07, 116.88, 116.77, 116.68, 116.55, 36.52, 36.33, 36.13, 15.90, 15.75, 15.73, 15.60, 15.58, 15.44; HRMS: calcd for $C_{12}H_{12}N_4O_2S_2$ $[M+H]^+$ 309.0480, found. 309.0473.

(*E*)-*N*'-(4-Methoxybenzylidene)-2-((5-methyl-1,3,4-thiadiazol-2-yl)thio)acetohydrazide (TEH09): White solid; yield = 81%, m.p.: 96-97 ºC; ATR-FTIR (ν, cm^{-1}, neat) 1655 (amide C=O str.), 1599 (C=N str.), 1379 (aromatic amine C-N str.), 1243 (amine C-N str.), 1207 (alkyl aryl ether C-O str.); ^{1}H NMR (500 MHz, $CDCl_3$) δ ppm 10.82 (s, 1H), 10.05 (s, 1H), 8.02 (s, 1H), 7.83 (s, 1H), 7.72 – 7.65 (m, 2H), 7.64 – 7.58 (m, 2H), 6.96 – 6.86 (m, 4H), 4.64 (s, 2H), 4.05 (s, 2H), 3.86 (s, 3H), 3.84 (s, 2H), 2.77 (s, 2H), 2.70 (s, 3H); ^{13}C NMR (126 MHz, $CDCl_3$) δ ppm 169.29, 166.51, 166.09, 165.63, 164.56, 164.40, 161.61, 161.49, 148.68, 148.61, 145.20, 145.13, 129.51, 129.01, 126.08, 126.04, 114.25, 114.10, 55.48, 55.43, 55.35, 55.31,

36.09, 35.40, 15.79, 15.70, 15.60; HRMS: calcd for $C_{13}H_{14}N_4O_2S_2$ $[M+H]^+$ 323.0636, found. 323.0632.

(*E*)-*N*'-(2,5-Dimethoxybenzylidene)-2-((5-methyl-1,3,4-thiadiazol-2-yl)thio)acetohydrazide (TEH10): White solid; yield = 98%, m.p.: 159-160 ºC; ATR-FTIR (ν, cm^{-1}, neat) 3191 (amide N-H str.), 3001 (aromatic C-H str.), 1694 (amide C=O str.), 1563 (C=N str.), 1367 (aromatic amine C-N str.), 1279 (amine C-N str.), 1217 (alkyl aryl ether C-O str.); ^{1}H NMR (500 MHz, $CDCl_3$) δ ppm 10.74 (d, *J* = 8.1 Hz, 1H), 8.46 (s, 1H), 8.24 (d, *J* = 3.8 Hz, 1H), 7.54 (t, *J* = 3.1 Hz, 1H), 7.40 (d, *J* = 3.1 Hz, 1H), 6.96 – 6.93 (m, 1H), 6.93 – 6.90 (m, 1H), 6.87 – 6.83 (m, 1H), 6.81 (d, *J* = 9.0 Hz, 1H), 4.62 (s, 2H), 4.07 (s, 2H), 3.82 (s, 6H), 3.81 (s, 2H), 3.79 (s, 2H), 2.77 (d, *J* = 2.4 Hz, 2H), 2.70 (s, 3H); ^{13}C NMR (126 MHz, $CDCl_3$) δ ppm 169.08, 166.19, 166.00, 165.67, 164.49, 164.44, 153.67, 152.86, 152.78, 144.83, 144.80, 141.16, 141.11, 122.32, 122.22, 119.30, 117.94, 112.54, 112.42, 110.29, 109.94, 109.90, 56.26, 56.19, 56.14, 56.08, 56.03, 55.92, 55.81, 55.69, 36.11, 35.42, 35.30, 15.77, 15.68, 15.58; HRMS: calcd for $C_{14}H_{16}N_4O_3S_2$ $[M+H]^+$ 353.0742, found. 353.0738.

(*E*)-2-((5-Methyl-1,3,4-thiadiazol-2-yl)thio)-*N*'-(3,4,5-trimethoxybenzylidene)acetohydrazide (TEH11): White solid; yield = 85%, m.p.: 168-169 ºC; ATR-FTIR (ν, cm^{-1}, neat) 1654 (amide C=O str.), 1574 (C=N str.), 1329 (aromatic amine C-N str.), 1226 (amine C-N str.), 1116 (alkyl aryl ether C-O str.); ^{1}H NMR (500 MHz, $CDCl_3$) δ ppm 10.96 (s, 2H), 10.00 (s, 1H), 8.02 (s, 2H), 7.80 (s, 1H), 6.97 (s, 4H), 6.91 (s, 3H), 4.65 (s, 3H), 4.04 (s, 4H), 3.92 (s, 6H), 3.90 (s, 4H), 3.89 (s, 9H), 3.88 (s, 5H), 2.79 (s, 5H), 2.70 (s, 4H); ^{13}C NMR (126 MHz, $CDCl_3$) δ ppm 169.30, 166.64, 166.19, 165.70, 164.55, 164.30, 153.53, 153.39, 148.86, 148.79, 145.24, 145.17, 140.20, 128.80, 128.73, 104.91, 104.85, 104.50, 104.43, 61.07, 61.02, 60.89,

56.36, 56.34, 56.23, 56.21, 56.10, 35.81, 35.58, 35.44, 15.81, 15.71, 15.60; HRMS: calcd for $C_{15}H_{18}N_4O_4S_2$ $[M+H]^+$ 383.0847, found. 383.0841.

(*E*)-*N*'-(4-Hydroxy-3-methoxybenzylidene)-2-((5-methyl-1,3,4-thiadiazol-2-yl)thio)acetohydrazide (TEH12): White solid; yield = 87%, m.p.: 142-144 ºC; ATR-FTIR (ν, cm^{-1}, neat) 1659 (amide C=O str.), 1595 (C=N str.), 1381 (aromatic amine C-N str.), 1268 (amine C-N str.), 1193 (phenolic C-O str.); ^{1}H NMR (500 MHz, DMSO-d_6) δ ppm 11.61 (s, 1H), 11.56 (s, 1H), 9.58 (s, 1H), 9.54 (s, 1H), 8.08 (s, 1H), 7.91 (s, 1H), 7.27 (d, *J* = 1.9 Hz, 2H), 7.09 (dt, *J* = 8.2, 1.8 Hz, 2H), 6.83 (d, *J* = 8.1 Hz, 2H), 4.56 (s, 2H), 4.14 (s, 1H), 3.82 (s, 3H), 3.81 (s, 2H), 2.68 (s, 2H), 2.66 (s, 3H); ^{13}C NMR (126 MHz, DMSO-d_6) δ ppm 168.38, 166.23, 166.03, 165.30, 164.75, 163.15, 149.54, 149.30, 148.46, 148.39, 148.23, 148.09, 144.82, 144.67, 125.81, 122.61, 121.78, 121.72, 116.07, 115.94, 110.12, 109.51, 56.13, 56.08, 55.93, 36.64, 36.32, 15.74, 15.72, 15.60, 15.57, 15.42; HRMS: calcd for $C_{13}H_{14}N_4O_3S_2$ $[M+H]^+$ 339.0585, found. 339.0581.

(*E*)-2-((5-Methyl-1,3,4-thiadiazol-2-yl)thio)-*N*'-(4-nitrobenzylidene)acetohydrazide (TEH13): White solid; yield = 97%, m.p.: 163-165 ºC; ATR-FTIR (ν, cm^{-1}, neat) 3087 (aromatic C-H str.), 1676 (amide C=O str.), 1583 (C=N str.), 1387 (aromatic amine C-N str.), 1514 (nitro str.), 1336 (nitro str.); ^{1}H NMR (500 MHz, DMSO-d_6) δ ppm 12.09 (s, 1H), 12.01 (s, 1H), 8.33 – 8.27 (m, 4H), 8.14 (s, 1H), 8.00 – 7.92 (m, 3H), 4.63 (s, 2H), 4.21 (s, 1H), 2.69 (s, 2H), 2.67 (s, 3H); ^{13}C NMR (126 MHz, DMSO-d_6) δ ppm 169.18, 166.29, 166.13, 164.96, 164.09, 148.27, 141.96, 140.85, 140.68, 128.66, 128.47, 128.28, 124.59, 124.45, 36.23, 15.75, 15.59; HRMS: calcd for $C_{12}H_{11}N_5O_3S_2$ $[M+H]^+$ 338.0381, found. 338.0375.

(*E*)-2-((5-Methyl-1,3,4-thiadiazol-2-yl)thio)-*N*'-(pyridin-3-ylmethylene)acetohydrazide (TEH14): White solid; yield = 98%, m.p.: 153-155 ºC; ATR-FTIR (ν, cm^{-1}, neat) 3208 (amide N-H str.), 3052 (aromatic C-H str.), 1665 (amide C=O str.), 1599 (C=N str.), 1549 (N-H bend.), 1382 (aromatic amine C-N str.); ^{1}H NMR (500 MHz, DMSO-d_6) δ ppm 11.95 (s, 1H), 11.88 (s, 2H), 8.88 – 8.83 (m, 3H), 8.61 (dt, *J* = 4.7, 2.1 Hz, 3H), 8.27 (s, 1H), 8.11 (ddt, *J* = 7.6, 3.8, 2.0 Hz, 3H), 8.07 (s, 2H), 7.51 – 7.44 (m, 3H), 4.61 (s, 4H), 4.19 (s, 2H), 2.69 (s, 3H), 2.67 (s, 6H); ^{13}C NMR (126 MHz, DMSO-d_6) δ ppm 168.96, 166.27, 166.09, 165.09, 164.62, 163.78, 151.11, 151.03, 149.31, 149.02, 145.07, 144.93, 141.65, 141.48, 134.02, 133.86, 130.43, 130.34, 124.46, 124.36, 36.56, 36.33, 15.89, 15.74, 15.58, 15.42; HRMS: calcd for $C_{11}H_{11}N_5OS_2$ $[M+H]^+$ 294.0483, found. 294.0487.

(*E*)-*N*'-(Furan-2-ylmethylene)-2-((5-methyl-1,3,4-thiadiazol-2-yl)thio)acetohydrazide (TEH15): White solid; yield = 83%, m.p.: 148-150 ºC; ATR-FTIR (ν, cm^{-1}, neat) 3186 (amide N-H str.), 3058 (aromatic C-H str.), 1669 (amide C=O str.), 1563 (C=N str.), 1382 (aromatic amine C-N str.), 1201 (alkyl aryl ether C-O str.), 984 (alkene C=C bend.); ^{1}H NMR (500 MHz, $CDCl_3$) δ ppm 10.93 (s, 1H), 10.01 (s, 1H), 8.08 (s, 1H), 7.78 (s, 1H), 7.52 (dt, *J* = 13.5, 1.2 Hz, 2H), 6.82 (d, *J* = 3.4 Hz, 1H), 6.76 (d, *J* = 3.5 Hz, 1H), 6.49 (ddd, *J* = 14.3, 3.5, 1.8 Hz, 2H), 4.61 (s, 2H), 4.04 (s, 2H), 2.78 (s, 3H), 2.72 (s, 2H); ^{13}C NMR (126 MHz, $CDCl_3$) δ ppm 169.37, 166.50, 166.11, 165.62, 164.58, 164.35, 148.96, 148.87, 144.90, 144.86, 144.76, 144.71, 138.50, 138.44, 134.99, 134.93, 113.88, 113.80, 113.59, 113.50, 112.04, 111.93, 35.83, 35.52, 35.40, 15.78, 15.68, 15.60; HRMS: calcd for $C_{10}H_{10}N_4O_2S_2$ $[M+H]^+$ 283.0323, found. 283.0320.

(*E*)-2-((5-Methyl-1,3,4-thiadiazol-2-yl)thio)-*N*'-(1-phenylethylidene)acetohydrazide (TEH16): White solid; yield = 93%, m.p.: 96-98 ºC; ATR-FTIR (ν, cm^{-1}, neat) 3196 (amide N-H str.), 3061 (aromatic C-H str.), 1667 (amide C=O str.), 1570 (C=N str.), 1382 (aromatic amine C-N str.); ^{1}H NMR (500 MHz, $CDCl_3$) δ ppm 10.89 (s, 1H), 8.88 (s, 1H), 7.85 – 7.81 (m, 2H), 7.79 – 7.75 (m, 2H), 7.46 – 7.41 (m, 3H), 7.41 – 7.35 (m, 3H), 4.68 (s, 2H), 4.07 (s, 2H), 2.79 (s, 3H), 2.73 (s, 3H), 2.37 (s, 3H), 2.27 (s, 2H); ^{13}C NMR (126 MHz, $CDCl_3$) δ ppm 169.27, 166.08, 165.52, 164.71, 164.44, 153.00, 148.55, 137.81, 137.36, 129.75, 129.62, 128.58, 128.33, 126.84, 126.77, 36.28, 35.42, 15.63, 14.53; HRMS: calcd for $C_{13}H_{14}N_4OS_2$ $[M+H]^+$ 307.0687, found. 307.0685.

(*E*)-*N*'-(1-(4-Fluorophenyl)ethylidene)-2-((5-methyl-1,3,4-thiadiazol-2-yl)thio)acetohydrazide (TEH17): White solid; yield = 85%, m.p.: 142-144 ºC; ATR-FTIR (ν, cm^{-1}, neat) 3193 (amide N-H str.), 1671 (amide C=O str.), 1599 (C=N str.), 1374 (aromatic amine C-N str.), 1203 (C-F str.); ^{1}H NMR (500 MHz, $CDCl_3$) δ ppm 10.91 (s, 1H), 9.09 (s, 1H), 7.86 – 7.81 (m, 2H), 7.81 – 7.72 (m, 2H), 7.15 – 7.02 (m, 4H), 4.67 (s, 1H), 4.06 (s, 2H), 2.79 (s, 3H), 2.73 (s, 2H), 2.35 (s, 3H), 2.25 (s, 2H); ^{13}C NMR (126 MHz, $CDCl_3$) δ ppm 169.37, 167.06, 166.12, 165.50, 164.75, 164.42, 162.74, 151.87, 147.67, 133.97, 133.57, 128.74, 128.68, 128.22, 115.64, 115.46, 115.38, 115.23, 36.22, 35.42, 35.28, 15.81, 15.70, 15.63, 14.51, 14.45, 12.99; HRMS: calcd for $C_{13}H_{13}FN_4OS_2$ $[M+H]^+$ 325.0593, found. 325.0562.

(*E*)-*N*'-(1-(4-Chlorophenyl)ethylidene)-2-((5-methyl-1,3,4-thiadiazol-2-yl)thio)acetohydrazide (TEH18): White solid; yield = 78%, m.p.: 156-158 ºC; ATR-FTIR (ν, cm^{-1}, neat) 3192 (amide N-H str.), 3096 (aromatic C-H str.), 1668 (amide C=O str.), 829 (C-Cl str.); ^{1}H NMR (500 MHz, $CDCl_3$) δ ppm 10.95 (s, 1H), 9.18 (s, 1H),

7.81 – 7.74 (m, 2H), 7.73 – 7.67 (m, 2H), 7.42 – 7.31 (m, 4H), 4.66 (s, 1H), 4.06 (s, 2H), 2.79 (s, 3H), 2.73 (s, 2H), 2.34 (s, 3H), 2.25 (s, 2H); ^{13}C NMR (126 MHz, $CDCl_3$) δ ppm 169.44, 167.06, 166.14, 165.52, 164.79, 164.38, 151.64, 147.58, 136.22, 135.85, 135.75, 135.66, 128.76, 128.54, 128.11, 128.05, 127.60, 36.18, 35.43, 15.81, 15.70, 14.35, 14.29, 12.90, 12.87; HRMS: calcd for $C_{13}H_{13}ClN_4OS_2$ $[M+H]^+$ 341.0297, found. 341.0289.

(*E*)-*N*'-(1-(4-Bromophenyl)ethylidene)-2-((5-methyl-1,3,4-thiadiazol-2-yl)thio)acetohydrazide (TEH19): White solid; yield = 88%, m.p.: 146-148 ºC; ATR-FTIR (*v*, cm^{-1}, neat) 3187 (amide N-H str.), 3091 (aromatic C-H str.), 1665 (amide C=O str.), 1387 (aromatic amine C-N str.), 608 (C-Br str.); ^{1}H NMR (500 MHz, DMSO-d_6) δ ppm 11.02 (s, 1H), 10.82 (s, 1H), 7.77 – 7.73 (m, 3H), 7.65 – 7.61 (m, 3H), 4.62 (s, 2H), 4.29 (s, 1H), 2.69 (s, 2H), 2.67 (s, 3H), 2.29 (s, 2H), 2.27 (s, 3H); ^{13}C NMR (126 MHz, $CDCl_3$) δ ppm 167.05, 166.11, 164.75, 151.68, 136.68, 131.75, 131.50, 128.33, 127.79, 124.06, 36.08, 35.44, 15.72, 15.65, 14.23, 12.64; HRMS: calcd for $C_{13}H_{13}BrN_4OS_2$ $[M+H]^+$ 384.9792, found. 384.9775.

(*E*)-*N*'-(1-(4-Hydroxyphenyl)ethylidene)-2-((5-methyl-1,3,4-thiadiazol-2-yl)thio)acetohydrazide (TEH20): White solid; yield = 54%, m.p.: 156-158 ºC; ATR-FTIR (*v*, cm^{-1}, neat) 3178 (amide N-H str.), 3019 (aromatic C-H str.), 1676 (amide C=O str.), 1379 (aromatic amine C-N str.), 1246 (phenolic C-O str.); ^{1}H NMR (500 MHz, DMSO-d_6) δ ppm 10.80 (s, 1H), 10.63 (s, 1H), 9.79 (s, 1H), 9.77 (s, 1H), 7.68 – 7.61 (m, 3H), 6.84 – 6.76 (m, 4H), 4.58 (s, 2H), 4.25 (s, 1H), 2.69 (s, 2H), 2.67 (s, 3H), 2.23 (s, 2H), 2.21 (s, 3H); ^{13}C NMR (126 MHz, DMSO-d_6) δ ppm 169.30, 166.27, 165.93, 165.43, 165.03, 163.73, 159.29, 159.14, 153.36, 149.25, 129.22, 128.29, 128.10,

115.69, 115.50, 37.12, 15.90, 15.74, 15.58, 14.09; HRMS: calcd for $C_{13}H_{14}N_4O_2S_2$ $[M+H]^+$ 323.0636, found. 323.0606.

(*E*)-2-((5-Methyl-1,3,4-thiadiazol-2-yl)thio)-*N*'-(1-(4-nitrophenyl)ethylidene)acetohydrazide (TEH21): White solid; yield = 81%, m.p.: 195-197 ºC; ATR-FTIR (ν, cm^{-1}, neat) 3190 (amide N-H str.), 3079 (aromatic C-H str.), 1662 (amide C=O str.), 1578 (C=N str.), 1513 (nitro str.), 1338 (nitro str.), 1379 (aromatic amine C-N str.); ^1H NMR (500 MHz, $CDCl_3$) δ ppm 11.22 (s, 1H), 8.92 (s, 1H), 8.31 – 8.26 (m, 1H), 8.26 – 8.21 (m, 2H), 8.04 – 7.98 (m, 2H), 7.97 – 7.91 (m, 1H), 4.70 (s, 1H), 4.08 (s, 2H), 2.80 (s, 3H), 2.75 (s, 1H), 2.42 (s, 3H), 2.32 (s, 1H); HRMS: calcd for $C_{13}H_{13}N_5O_3S_2$ $[M+H]^+$ 352.0538, found. 352.0515.

4.3.2. Biological studies

4.3.2.1. *In vitro* SHP2 inhibition assay

In order to derive some inference on the target-oriented pharmacological potential of our synthesized compounds, they were evaluated for their in vitro SHP2 inhibitory ability. The SHP2 IC_{50} of the final compounds **TEH01-TEH21** are provided in **Table 4.3**. All compounds of this series displayed SHP2 IC_{50} in submicromolar to micromolar range with values from 0.120 ± 0.006 µM to 1.725 ± 0.026 µM. A general analysis of the correlation between structure and activity of the compounds shows that halogen substitution leads to increase in potency as compared to the unsubstituted ones. Also, substitution at the para position (i.e., R_1) was beneficial for activity of the final compound against SHP2 as compared to the ortho or meta substituted ones.

Table 4.3. *In vitro* SHP2 inhibition data of compounds **TEH01-TEH21**

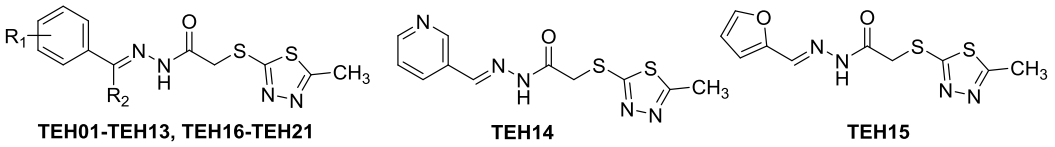

TEH01-TEH13, TEH16-TEH21 **TEH14** **TEH15**

R_2 = H (Aldimines, Group-I)
R_2 = CH_3 (Ketimines, Group-II)

Compd Code	R_1	R_2	SHP2 IC_{50} (μM)[a]	Compd Code	R_1	R_2	SHP2 IC_{50} (μM)[a]
TEH01	H	H	0.756 ± 0.023	**TEH12**	3-OMe-4-OH	H	0.787 ± 0.003
TEH02	4-Cl	H	1.252 ± 0.009	**TEH13**	4-NO_2	H	1.025 ± 0.002
TEH03	2-Cl	H	0.933 ± 0.005	**TEH14**	-	-	0.843 ± 0.004
TEH04	2,3-Cl_2	H	0.982 ± 0.001	**TEH15**	-	-	0.981 ± 0.005
TEH05	2,4-Cl_2	H	0.540 ± 0.018	**TEH16**	H	CH_3	1.725 ± 0.026
TEH06	2,6-Cl_2	H	0.120 ± 0.006	**TEH17**	4-F	CH_3	0.953 ± 0.006
TEH07	4-OH	H	1.009 ± 0.002	**TEH18**	4-Cl	CH_3	0.794 ± 0.003
TEH08	2-OH	H	1.116 ± 0.001	**TEH19**	4-Br	CH_3	0.890 ± 0.008
TEH09	4-OMe	H	0.696 ± 0.015	**TEH20**	4-OH	CH_3	0.737 ± 0.002
TEH10	2,5-di-OMe	H	0.934 ± 0.002	**TEH21**	4-NO_2	CH_3	1.144 ± 0.024
TEH11	3,4,5-tri-OMe	H	0.996 ± 0.012	**SHP099**	-	-	0.070[b]

[a] Values represent the assay drug concentration that give 50% inhibition of SHP2 activity and are the mean ± SEM of two independent experiments done in duplicate; statistical significance: $p<0.05$ versus the corresponding IC_{50} values obtained against SHP2, as determined by ANOVA/Dunnett's test. [b] Reported IC_{50} value against SHP2 in a comparable DiFMUP assay protocol using fl-SHP2 enzyme and a bis-tyrosyl phosphorylated peptide activator [94].

SAR of SHP2 inhibition for compounds TEH01-TEH21

The test compounds of this series can be classified into two groups based on the substitution at the imine carbon (R_2, **Figure 4.6**). The first group (Group-I i.e., aldimines; compounds **TEH01** to **TEH15**) is derived from reaction of the intermediate hydrazone (**IM04**) with suitable aromatic aldehydes (R_2 = H) whereas Group-II (ketimines; compounds **TEH16** to **TEH21**) is derived from reaction of the hydrazone (**IM04**) with aromatic ketones viz. substituted acetophenones (R_2 = CH_3). Within each group, the IC_{50} values show a clear picture of the effect of various substituents on the

activity of the compounds against SHP2. In compounds of Group-I, mono-halo substitution at both ortho or para position of the phenyl ring (R_1 = 2-Cl or 4-Cl) resulted in a surprising loss of activity from the unsubstituted derivative by almost 1.4-fold to 1.6-fold [compare, compounds **TEH02** (SHP2 IC_{50} = 1.252 ± 0.009 μM) and **TEH03** (SHP2 IC_{50} = 0.933 ± 0.005 μM) with **TEH01** (SHP2 IC_{50} = 0.756 ± 0.023 μM)].

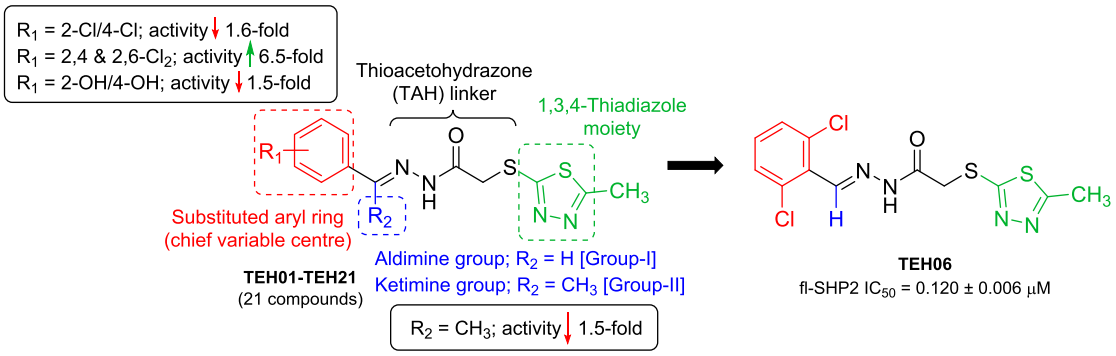

Figure 4.6. Major variable centres in the pharmacophore of the current series (shown in red, green and blue) and the activated *S*-acyl hydrazone linker (black) shown along with few salient SAR points (in boxes) and the skeletal formula of the *in vitro* lead SHP2 inhibitor, compound **TEH06**. The SAR points are all in comparison with the corresponding unsubstituted derivative i.e., R_1 & R_2 = H.

However, dichloro substitution enhanced activity manifold, particularly the 2,4-dichloro (compound **TEH05**, SHP2 IC_{50} = 0.540 ± 0.018 μM) and the 2,6-dichloro derivatives (compound **TEH06**, SHP2 IC_{50} = 0.120 ± 0.006 μM). In fact, **TEH06** emerged as the most potent SHP2 inhibitor of this group and also, among all compounds reported herein. This advantageous effect of the dichloro substitution may be attributed to the additional electronegativity that the two chlorine atoms bring to the molecule. Also, the position of the di-substitution is important for optimum activity as the 2,6-substitution leads to a molecule that imparts high electronegative potential to the attached carbohydrazone moiety.

Substitution with hydroxy group at *ortho* or *para* position resulted in considerable reduction in activity (compare compound **TEH07**, SHP2 IC_{50} = 1.009 ± 0.002 μM and compound **TEH08**, SHP2 IC_{50} = 1.116 ± 0.001 μM with compound **TEH01**). Increase in polarity and subsequent decrease in lipophilicity in our scaffold was thus detrimental to SHP2 inhibition. Activity, however, was somewhat restored on methylation of the *p*-hydroxy group i.e., for the 4-methoxy substituted product (compound **TEH09**, SHP2 IC_{50} = 0.696 ± 0.015 μM) owing to augmentation in the *+I* effect. Multiple methoxy substitutions, that too in the *ortho* and *meta* positions (compounds **TEH10**, SHP2 IC_{50} = 0.934 ± 0.002 μM and compound **TEH11**, SHP2 IC_{50} = 0.996 ± 0.012 μM) progressively reduced potency probably due to increased steric demand and reversal of the electronegative tendency. The corresponding vanillin derivative (compound **TEH12**, SHP2 IC_{50} = 0.787 ± 0.003 μM) maintained potency by exploiting the inductive and electromeric effect of the *p*-OH group. Replacement of the phenyl ring with heterocyclic ring like 3-pyridyl (compound **TEH14**, SHP2 IC_{50} = 0.843 ± 0.004 μM) or 2-furyl (compound **TEH15**, SHP2 IC_{50} = 0.981 ± 0.005 μM) did not cause any notable change in activity of the resultant analogue.

In compounds of Group-II, introduction of the imine methyl group (i.e., $R_2 = CH_3$) was largely responsible for reduction of SHP2 inhibitory activity as seen in compounds **TEH16** to **TEH21** with SHP2 IC_{50} values ranging from 0.737 ± 0.002 μM to 1.725 ± 0.026 μM. Within the group, the effect of different *para*-substitutions on the aryl ring was studied and we found that any substitution at the *para*-position lead to better inhibitory potential of the analogue. The 4-chloro derivative (compound **TEH18**, SHP2 IC_{50} = 0.794 ± 0.003 μM) was one of the more potent ones whereas the most potent compound of this group was found to be compound **TEH20** having a 4-OH group

(SHP2 IC_{50} = 0.737 ± 0.002 μM). Thus, it can be inferred that the presence of electron withdrawing groups on the aryl ring favour inhibition of SHP2 enzyme.

4.3.2.2. Cell-based study

4.3.2.2.1. Cell proliferation assay using MTT

Upon successfully evaluating the synthesized compounds of the series for their *in vitro* SHP2 inhibitory potential, they were further assessed for their antiproliferative effect using a cell proliferation/cytotoxicity assay in human breast cancer cell lines viz. MCF-7 using MTT and docetaxel as the reference standard. Potent SHP2 inhibiting small molecules have been shown to decrease the proliferation and viability of MCF-7 cells by *in vitro* assays [100]. The current library of compounds showed moderate to low antiproliferation or cytotoxic effect as seen in **Table 4.4**. Compound **TEH06**, which incidentally is our *in vitro* enzymatic lead, emerged as the most potent antiproliferative agent for MCF-7 cells with a best-in-library IC_{50} of 86.46 ± 2.32 μM and a 56% cell death at a concentration of 100 μM, followed by compound **TEH19** with an IC_{50} of 87.03 ± 2.28 μM. Unfortunately, most other compounds of the series displayed poor cytotoxicity with the IC_{50} values being >100 μM suggesting weak effect on the proliferation of MCF-7 cells. As seen from **Figure 4.7**, the two most cytotoxic compounds i.e., compounds **TEH06** and **TEH19** displayed dose-dependent cytotoxicity for MCF-7 cells; however, the dose-dependence was different from the standard, i.e., docetaxel (**Figure 4.7D**) where potent cell death is observed within a dose of 10 μM which attains a steady state equilibrium on increasing the concentration of docetaxel further. In the case of test compound **TEH06**, there is a steady increase in cell death with increasing concentration which does not reach 50% until after a test concentration of ca. 85 μM (**Figure 4.7A**).

Morphological changes in the MCF-7 cells were visualized by inverted microscopy after incubating the cells with compound **TEH06** at different concentrations for 24 h and is shown in **Figure 4.7B**. There was significant loss of healthy & morphologically intact cells upon treatment with the test compound in a dose dependent manner with gradually increasing dead cells with increasing dose of the compound. In fact, while some healthy cells could be seen at 10 μM (the lowest) or 70 μM (the median) concentration of compound **TEH06**, at the highest dose of 130 μM, no cells were intact and there was appearance of apoptotic bundles and necrotic cell debris. Thus, the microscopic visualization directly corroborates our findings regarding the dose-dependent cytotoxicity of compound **TEH06** for MCF-7 cells.

Table 4.4. MCF-7 cell growth inhibition data of compounds **TEH01-TEH21**

Compd Code	MCF-7 IC_{50} (μM)[a]	% MCF-7 Cell Death @ 100 μM	Compd Code	MCF-7 IC_{50} (μM)[a]	% MCF-7 Cell Death @ 100 μM
TEH01	366.40 ± 7.14	21.62	**TEH12**	422.17 ± 2.52	20.08
TEH02	202.33 ± 2.55	32.07	**TEH13**	314.90 ± 2.51	24.61
TEH03	118.78 ± 3.15	44.28	**TEH14**	141.32 ± 1.24	42.39
TEH04	258.60 ± 3.31	28.02	**TEH15**	379.44 ± 1.32	21.13
TEH05	192.65 ± 3.51	36.35	**TEH16**	290.52 ± 4.29	25.69
TEH06	86.46 ± 2.32	56.13	**TEH17**	175.67 ± 1.51	37.85
TEH07	393.21 ± 5.23	20.37	**TEH18**	288.06 ± 6.13	25.61
TEH08	333.34 ± 4.17	23.94	**TEH19**	87.03 ± 2.28	55.61
TEH09	>1000	NA	**TEH20**	919.38 ± 2.69	10.44
TEH10	311.59 ± 9.32	25.98	**TEH21**	263.11 ± 2.74	27.29
TEH11	156.93 ± 3.16	39.31	**Docetaxel**[b]	4.84 ± 0.16	91.72[c]

[a] Values represent the assay drug concentration that give 50% growth inhibition of MCF-7 cells and are the mean ± SD of two independent experiments done in triplicate; [b] Docetaxel used as internal standard; [c] % MCF-7 cell death at 50 μM concentration

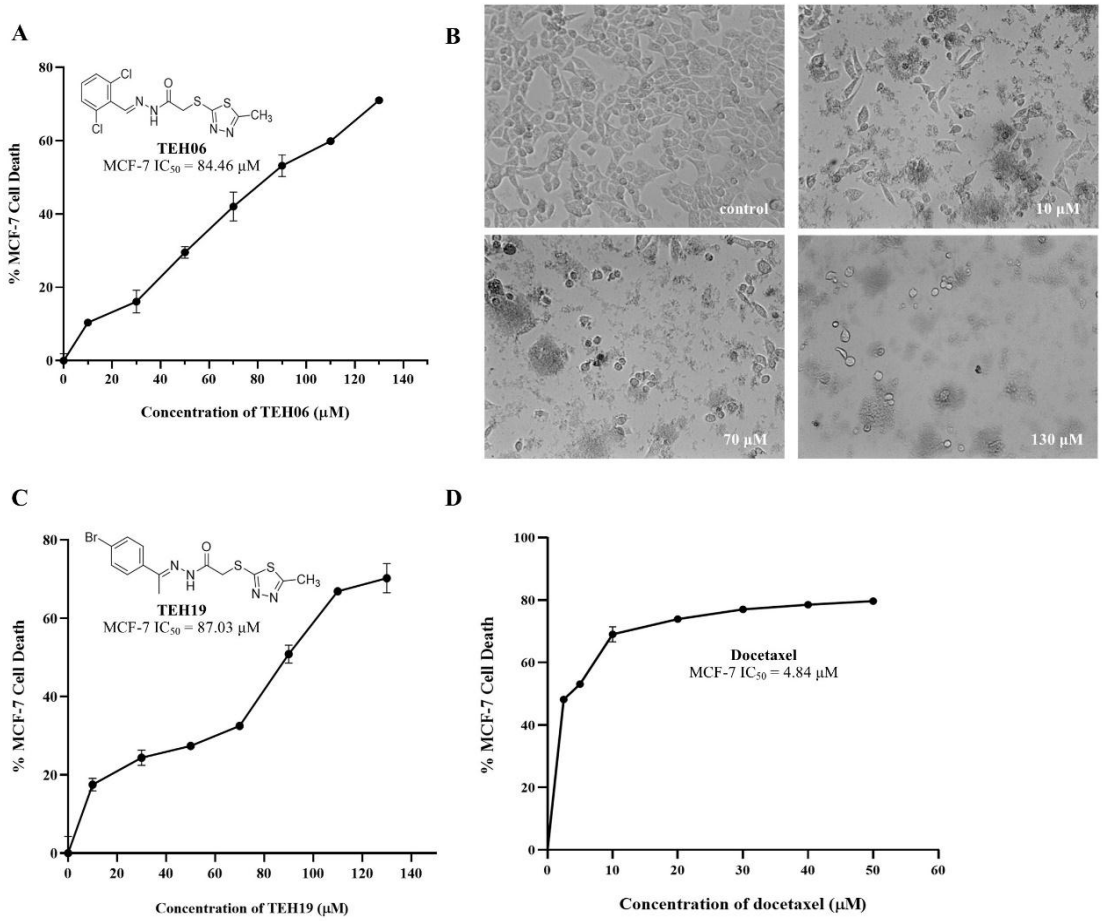

Figure 4.7. A) Percent MCF-7 cell death vs. concentration graph of compound **TEH06** after 24 h incubation post treatment; B) Inverted microscopic image of MCF-7 cells 24 h post treatment with compound **TEH06** at 0 µM (control), 10 µM, 70 µM and 100 µM concentrations; C) Percent MCF-7 cell death vs. concentration graph of compound **TEH19** after 24 h incubation post treatment; D) Percent MCF-7 cell death vs. concentration graph of docetaxel (reference standard) after 24 h incubation post treatment. Data are expressed as mean of assay in triplicate (n = 3).

4.3.2.2.2. Colony formation and scratch wound healing assay of compounds TEH06 and TEH19

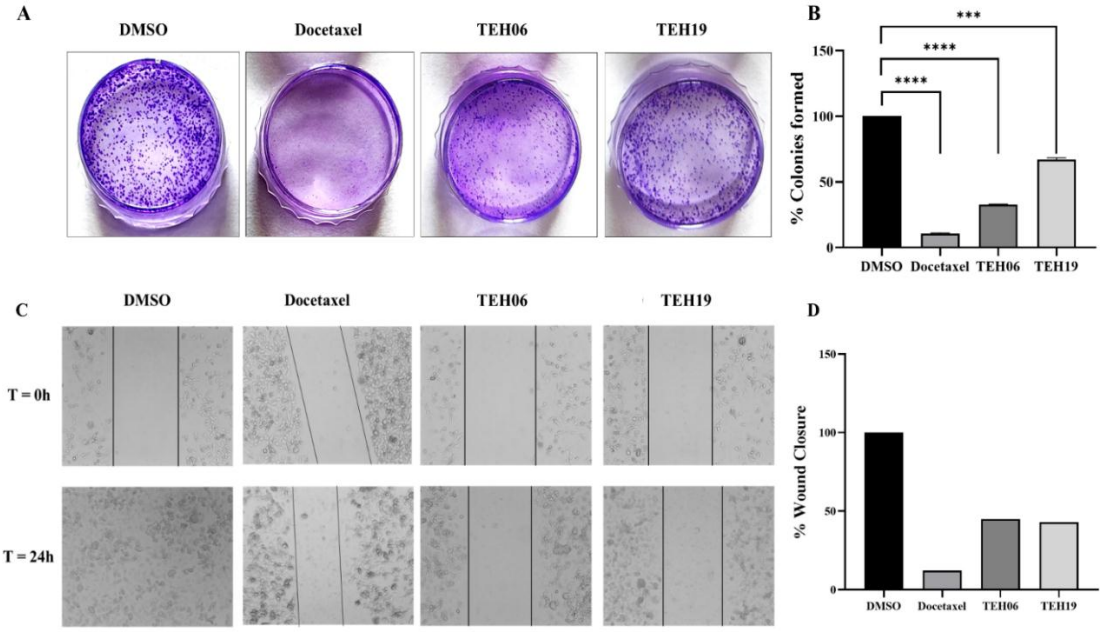

Figure 4.8. A) Inhibition of colony formation of MCF-7 cells by compounds **TEH06** & **TEH19** and docetaxel (reference standard) as compared to untreated cells (DMSO control) after an incubation of 7 days. B) Histogram quantifying the % colony formed (n = 3). ** $P < 0.01$, *** $P < 0.001$ versus DMSO. C) Inhibition of migration of MCF-7 cells by compounds **TEH06** & **TEH19** and docetaxel (reference standard) as compared to untreated cells (DMSO control) at 0 h and 24 h (magnification, 4x). D) Histogram quantifying the % migration.

The anti-survival and antimigratory effects was assessed for compounds **TEH06** and **TEH19** i.e., those two compounds which exhibited best-in-library *in vitro* cytotoxicity, using colony formation assay [155] and scratch wound healing assay [128] respectively in MCF-7 cells. In both the assays, docetaxel was used as the internal standard. Both the compounds exhibited considerable inhibition of colony growth of MCF-7 cells upon an incubation of 7 days and subsequent crystal violet staining (**Figure 4.8A**). Treatment with 5 μM of each compound resulted in a significant decrease in the clonogenic number (33% and 68% colony formation at the end of the experiment for compounds

TEH06 and **TEH19** respectively; 10% colony formation with docetaxel) and formation rate of MCF-7 cells (**Figure 4.8B**). Similarly, it was found that compounds **TEH06** and **TEH19** inhibited migration of MCF-7 cells and caused visible healing of the scratch wound as shown in **Figure 4.8C** [156]. Treatment with 5 μM of compounds **TEH06** and **TEH19** caused 45% and 43% closure of the scratch wound respectively after a period of 24 h (12.2% wound closure for docetaxel) hence indicating their acceptable anti-migratory effect in sub-IC_{50} dose (**Figure 4.8D**).

4.3.2.3. *In vivo* studies

4.3.2.3.1. Acute oral toxicity study in female albino mice

The *in vivo* safety of compound **TEH06** was evaluated by conducting an acute oral toxicity study on adult female albino mice in accordance with the OECD Guideline 423 (Acute Toxic Class Method). No animal was found dead or in moribund state within or after 14 days at the highest dose of 2000 mg/kg body weight (BW) indicating compound **TEH06** was safe for all the animals with its LD_{50} being >2000 mg/kg. Further, no external signs of toxicity were observed in any animal nor in the first 4 h post dosing neither in the subsequent 14 days; the vital signs and behavioural pattern of all groups were also normal.

Table 4.5. General observation and behavioural analysis during the first 4 h and 24 h after single-dose administration of compound **TEH06** (300 mg/kg and 2000 mg/kg BW) in albino mice (n = 6 female mice/group).

Observations	Control		TEH06 (300 mg/kg)		TEH06 (2000 mg/kg)	
	4 h	24 h	4 h	24 h	4 h	24 h
Skin and fur	NC	NC	NC	NC	NC	NC
Eyes	NC	NC	NC	NC	NC	NC
Mucous membrane	NC	NC	NC	NC	NC	NC
Salivation	NC	NC	NC	NC	NC	NC
Diarrhoea	NO	NO	NO	NO	NO	NO
Lethargy	NO	NO	NO	NO	NO	NO
Sleep	N	N	N	N	N	N
Coma	NO	NO	NO	NO	NO	NO
Tremors and convulsions	NO	NO	NO	NO	NO	NO
Behaviours pattern & somatosensory activity	N	N	N	N	N	N

Note: N-Normal, NO-Not observed, and NC-No change.

The body weight and food intake of the animals in all the test and control groups were determined and statistical analysis by two-way ANOVA revealed no significant differences in the body weight among the groups ([$F(2,45) = 4.019$; $p > 0.05$]), time ([$F(2,45) = 3.103$; $p > 0.05$]) and their interaction ([$F(4,45) = 0.3125$; $p > 0.05$]). Similarly, on 7^{th} and 14^{th} day, upon statistical analysis by two-way ANOVA no significant differences were revealed in food intake among the test groups ([$F(2,45) = 0.7905$; $p > 0.05$]), time ([$F(2,45) = 4.667$; $p > 0.05$]) and their interaction ([$F(4,45) = 0.04797$; $p > 0.05$]). Additionally, on the 7^{th} and 14^{th} day, assessment of neurobehavioral safety of compound **TEH06** was done by analysing its effects on spontaneous locomotor activity using an actophotometer. No significant changes were observed in any of the parameters evaluated in this test. In addition, the total distance covered by the female mice (track plot shown in **Figure 4.10**) corroborated the spontaneous locomotor activity observed in the actophotometer test.

The effect of single-dose oral administration of compound **TEH06** on the organ coefficient of vital organs i.e., brain, heart, liver, kidneys and spleen were determined post sacrifice of the animals and is depicted in **Figure 4.9C**. From the figure we can see

that the compound does not cause any significant changes in the organ coefficient of these highly perfused organs in any of the groups (statistical analysis by one-way ANOVA revealed no significant changes in the organ coefficient of brain, heart, liver, kidneys, and spleen among the groups; [$F(2,17) = 3.114$; $p > 0.05$], [$F(2,17) = 1.556$; $p > 0.05$], [$F(2,17) = 1.410$; $p > 0.05$], [$F(2,17) = 3.078$; $p > 0.05$], and [$F(2,17) = 0.4064$; $p > 0.05$] respectively) indicating that compound **TEH06** is safe for the organs even at the highest test dose of 2000 mg/kg BW.

Furthermore, the macroscopic evaluation of the said organs of all groups was done and we found no apparent signs of morphological damage or abnormalities in the organs of the test groups when compared to the vehicle control. **Figure 4.9B** shows the perfused organs of all three groups where even the highest dose of 2000 mg/kg BW did not show any toxicological effects. Also, a single oral administration of a dose of 300 mg/kg BW and 2000 mg/kg BW of compound **TEH06** exhibited no damage to the tissue architecture of the brain, liver, heart, spleen and the kidneys with no histopathological changes in any of these highly perfused organs at the end of the experiment i.e., on the 14^{th} day (**Figure 4.11**).

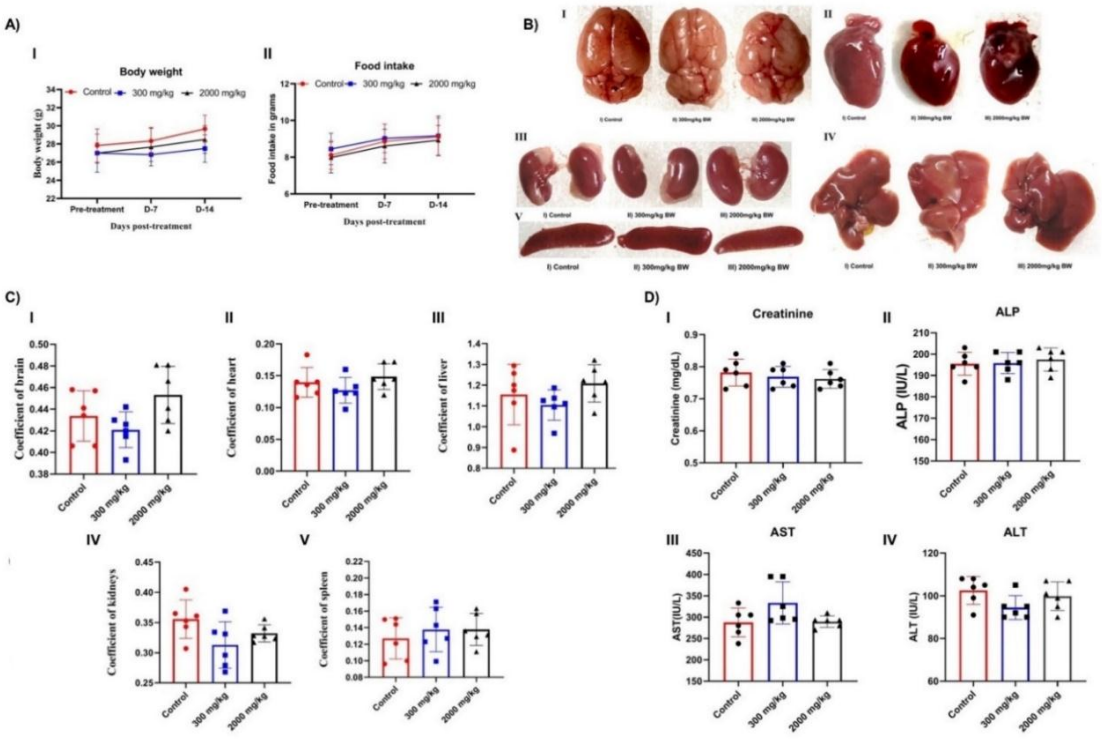

Figure 4.9. Acute oral toxicity study of compound **TEH06** in adult female albino mice (in accordance with OECD Guidelines 423). A) Effect of single-dose oral administration of compound **TEH06** (at two doses of 300 mg/kg BW and 2000 mg/kg BW) on (I) body weight and (II) food intake of rats at pre-treatment, Day-7 and Day-14. (Two-way ANOVA followed by Bonferroni post hoc test). B) Representative macroscopic photographs showing normal morphology of brain (I), heart (II), kidneys (III), liver (IV) and spleen (V) of animals after single-dose administration of vehicle (control) and 300 mg/kg BW & 2000 mg/kg BW of compound **TEH06** at the end of day 14. C) Effect of single-dose oral administration of compound **TEH06** (300 mg/kg BW and 2000 mg/kg BW) on organ coefficient of the brain (I), heart (II), liver (III), kidneys (IV), and spleen (V) at the end of the experiment. D) Effect of single-dose oral administration of compound **TEH06** (300 mg/kg BW and 2000 mg/kg BW) on serum concentration of creatinine (I), ALP (II), AST (III) and ALT (IV) at the end of the experiment. All values are in mean ± SD (n = 6 female mice/group). (One-way ANOVA followed by Tukey's multiple comparison post hoc test).

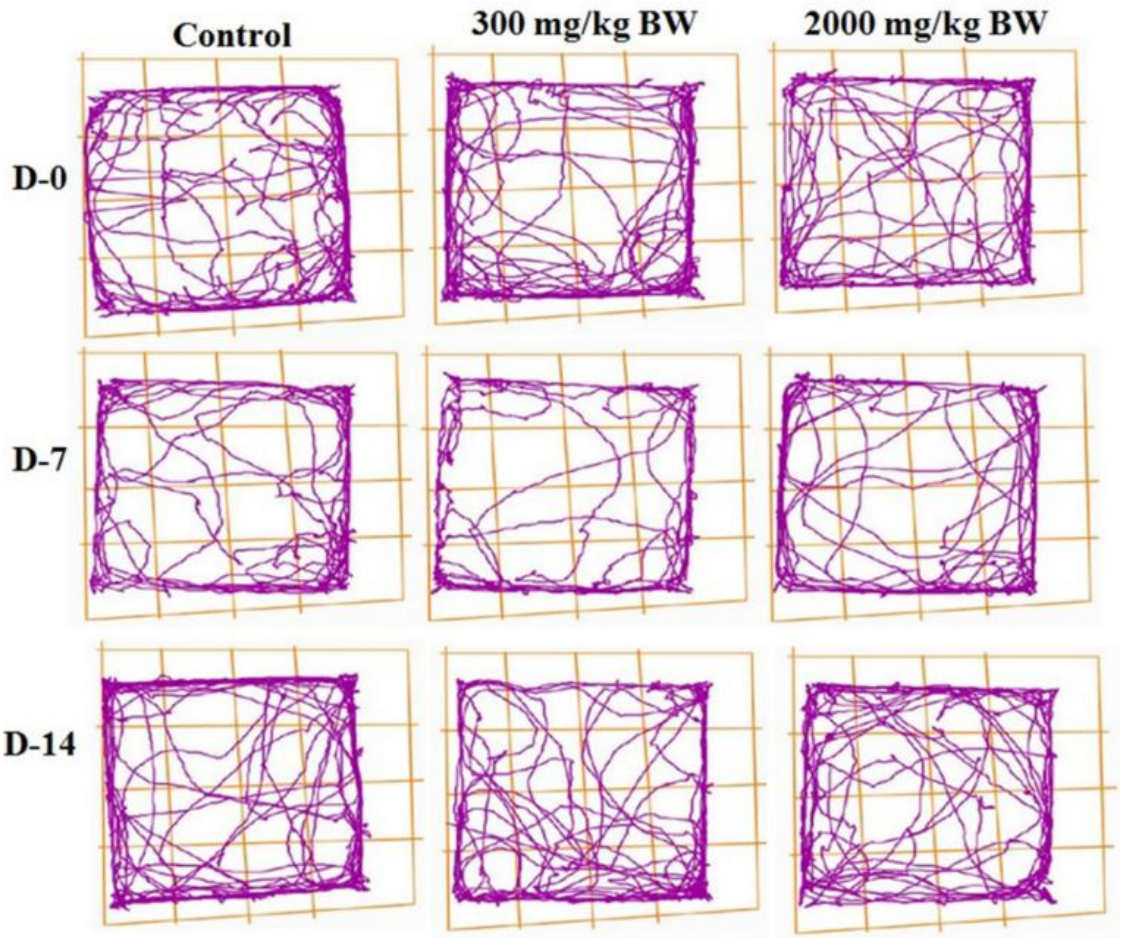

Figure 4.10. Schematic representation of the track plot of control, compound **TEH06** (300 mg/kg BW and 2000 mg/kg BW), treated mice recorded during 5 min test sessions on day 14 using ANY-maze behavioral tracking software.

All measurements and statistical data of the biochemical measurements for serum creatinine (mg/dL), ALP (IU/L), AST (IU/L) and ALT (IU/L) are shown in **Figure 4.9D**. We can observe from the figure that there were no substantial changes in the serum level of the enzymes in any of the groups when compared to control (statistical analysis by one-way ANOVA revealed no significant changes in the serum level of creatinine, AST, ALT, and ALP among the groups; [$F(2,17) = 0.5114$; $p > 0.05$], [$F(2,17) = 3.202$; $p > 0.05$], [$F(2,17) = 2.506$; $p > 0.05$], and [$F(2,17) = 0.2485$; $p > 0.05$] respectively). Lastly, complete blood count (CBC) of all the test groups was done

to check for any toxicological effect of compound **TEH06** on the haematology of the animals.

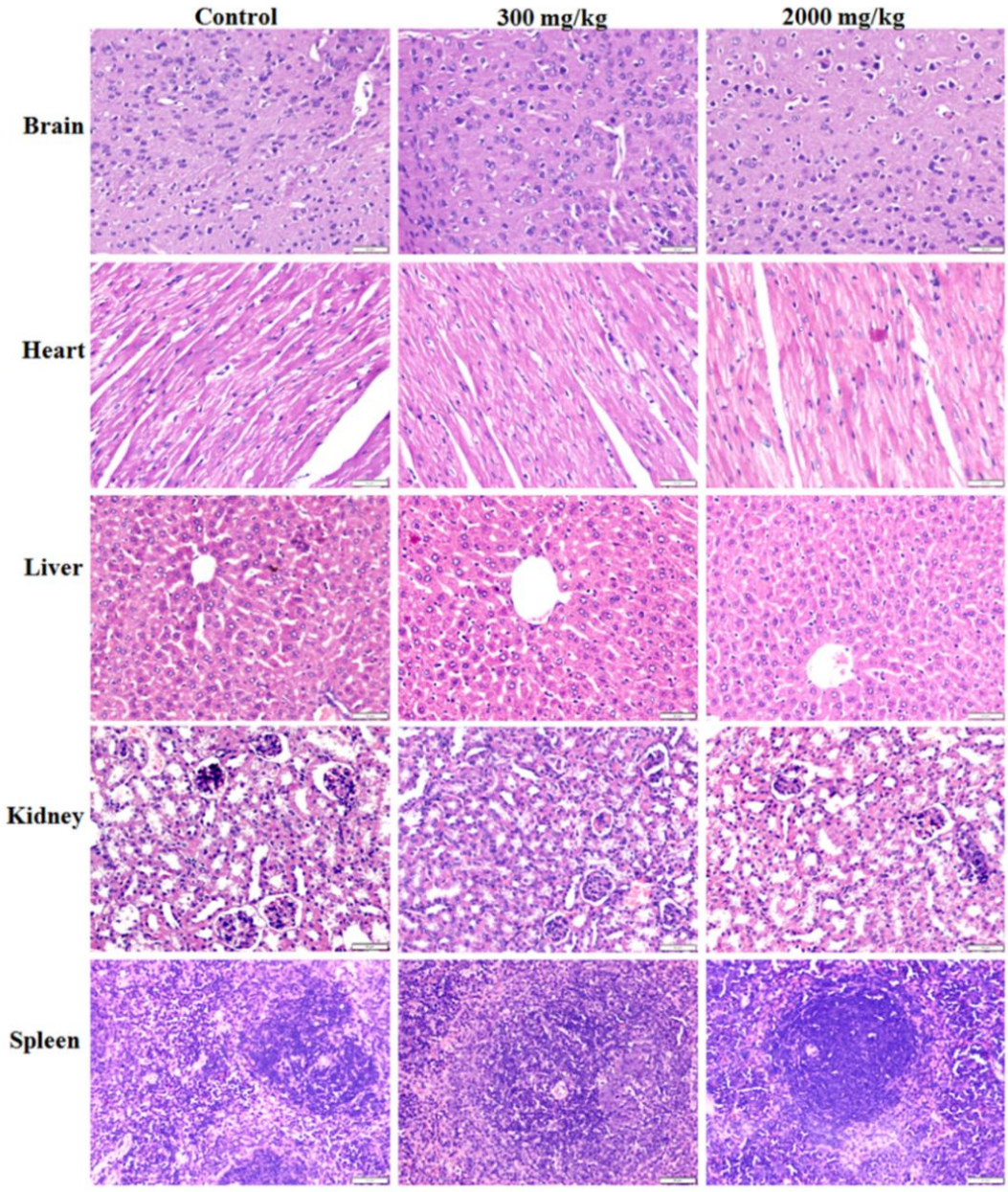

Figure 4.11. Effect of single-dose oral administration of compound **TEH06** (at two doses of 300 mg/kg BW and 2000 mg/kg BW) along with vehicle control on highly perfused organs of female albino mice viz. brain, heart, liver, kidney, and spleen tissue stained with hematoxylin and eosin (H&E)**.**

The estimated values of the haematological parameters (hemoglobin, red blood cell count (RBC), hematocrit (HCT), mean corpuscular hemoglobin (MCH), mean

corpuscular volume (MCV), mean corpuscular hemoglobin concentration (MCHC), red blood cell distribution width (RDW), platelet count and white blood cell count (WBC), **Figure 4.12**) after single-dose oral administration of compound **TEH06** showed no significant changes or deviations from the control group. From the above findings of the toxicological study, we inferred that compound **TEH06** is nontoxic and safe at the high oral dose of 2000 mg/kg BW.

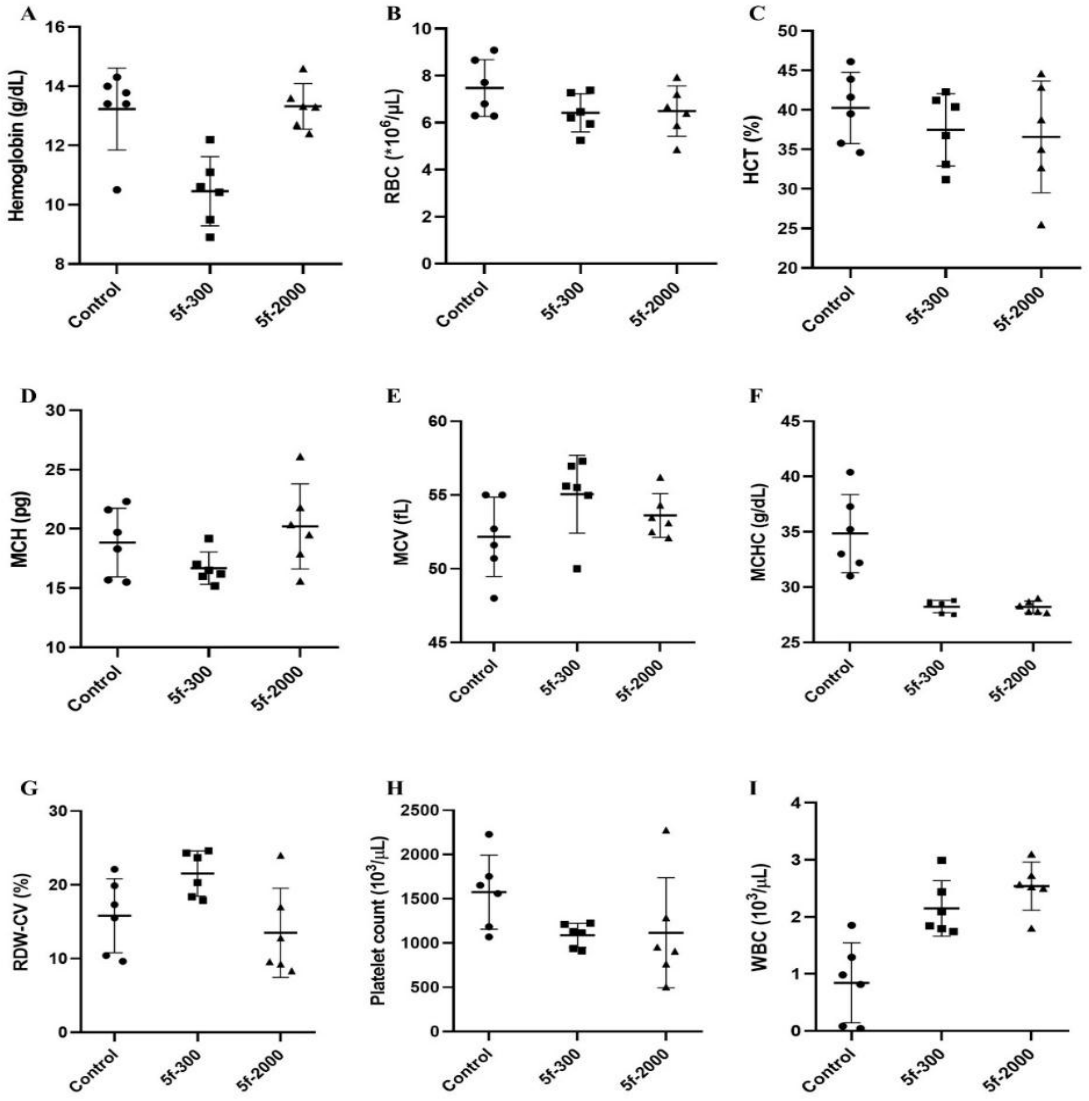

Figure 4.12. Effect of single-dose oral administration of compound **TEH06** (300 and 2000 mg/kg BW) on hemoglobin (A), total RBC count (B), HCT (C), MCH (D), MCV (E), MCHC (F), RDW (G), platelet count (H), and WBC (I) of female albino mice at

the end of 14-day experimental protocol. All values are in mean ± SD (n=6 female mice/ group). (One-way ANOVA followed by Tukey's multiple comparison post hoc test)

4.3.3. Computational studies

4.3.3.1. Molecular docking of compounds TEH01-TEH21 within the tunnel allosteric site of SHP2 (PDB ID: 5EHR)

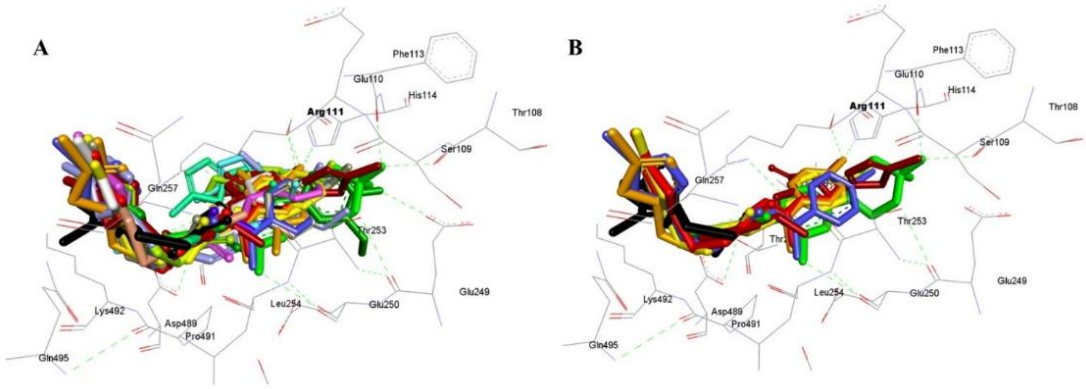

Figure 4.13. Superimposed image of compounds **TEH01-TEH21** with **SHP099** within the tunnel allosteric site of SHP2 (PDB ID: 5EHR). A) Cluster image of compounds **TEH01** (red), **TEH02** (blue), **TEH03** (yellow), **TEH04** (light blue), **TEH05** (pink), **TEH06** (orange), **TEH07** (black), **TEH08** (brown), **TEH09** (grey), **TEH10** (light green), **TEH11** (light purple), **TEH12** (moss green), **TEH13** (light pink), **TEH14** (white), **TEH15** (sea green) and **SHP099** (green). B) Cluster image of compounds **TEH16** (brown), **TEH17** (red), **TEH18** (blue), **TEH19** (yellow), **TEH20** (orange) and **TEH21** (black) with **SHP099** (green).

All *in vitro* enzymatic SHP2 inhibitory results obtained for our synthesized compounds **TEH01-TEH21** were verified by *in silico* methods to further gain virtual insights into the interaction patterns of the compounds with SHP2. All the docked molecules of our series were divided into two clusters according to the R_2 group as mentioned above (**Figure 4.13A** is for the aldimines, R_2 = H; **Figure 4.13B** is for the ketimines, R_2 = CH_3). The cluster images show that all molecules of the series occupied the desired binding site with the substituted phenyl ring orienting itself and interacting with the catalytic triad; the moiety also overlaid precisely with the piperidinyl ring of **SHP099**.

Table 4.6. Molecular docking data of compounds **TEH01-TEH21**

Compd code	ΔG (Kcal/mol)	Calc. K_i[a] (nM)	Compd code	ΔG (kcal/mol)	Calc. K_i[a] (nM)
TEH01	-8.45	0.639	**TEH12**	-7.28	4.594
TEH02	-7.91	1.580	**TEH13**	-8.68	0.437
TEH03	-8.31	0.813	**TEH14**	-7.53	3.03
TEH04	-8.44	0.655	**TEH15**	-7.86	1.74
TEH05	-8.39	0.704	**TEH16**	-8.43	0.663
TEH06	-8.55	0.537	**TEH17**	-8.29	0.833
TEH07	-7.29	4.512	**TEH18**	-8.67	0.443
TEH08	-7.00	7.464	**TEH19**	-8.60	0.498
TEH09	-7.54	2.96	**TEH20**	-8.07	1.22
TEH10	-8.70	0.422	**TEH21**	-8.69	0.425
TEH11	-8.14	1.072	**SHP099**	-10.27	29.34

[a] K_i calculated from the binding energy of poses generated by AutoDockTools 4.2.

Table 4.6 lists the binding energy (ΔG, kcal/mol) and the calculated virtual inhibition constants (K_i, μM) of the docked molecules from where we can observe that compound **TEH10** emerged as the virtual lead molecule with a binding energy of -8.70 kcal/mol and a calculated K_i of 0.422 μM for 5EHR. Our *in vitro* lead i.e., compound **TEH06** also displayed strong affinity for SHP2 tunnel allosteric site (ΔG = -8.55 kcal/mol, calc. K_i = 0.537 μM). A study of the 2D and 3D interaction images of these two compounds revealed many interactions with the key amino acid residues of the binding site, i.e., Arg111, Phe113 and Glu250 (**Figure 4.14A-D**).

A. Binding data of compound TEH10 within the crystal structure of 5EHR

A study of the 2D and 3D interaction diagram of compound **TEH10** (Figure **4.14A** and **4.14B**) revealed many crucial interactions of the molecule with Arg111, the key member of the tunnel allosteric catalytic triad. The ligand occupied the cavity lined by

the three residues of the catalytic triad and most of the molecule overlapped with **SHP099**. The thiadiazole moiety was oriented away from the binding cavity; however, the ring interacted with Arg111 via pi-cation bonds. Arg111 showed multiple interactions with the ligand via conventional H-bond (with one of the phenyloxy oxygen), pi-donor H-bond (with the other phenyloxy oxygen) and tethers & stabilizes the conformation of the molecule with a multidentate approach. The central role played by Arg111 in orienting the ligand in its most stable and low energy conformation within the tunnel allosteric site of SHP2 makes the ligand achieve the best binding affinity for the enzyme. Other important interactions are displayed by the terminal methoxy carbon atom of the molecule with Glu 110 & Phe113 (both by pi-donor H-bonds), and a unique alkyl interaction with His114. Thus, presence of the 2,5-dimethoxy group increases the quantum of interactions of the ligand with the enzyme.

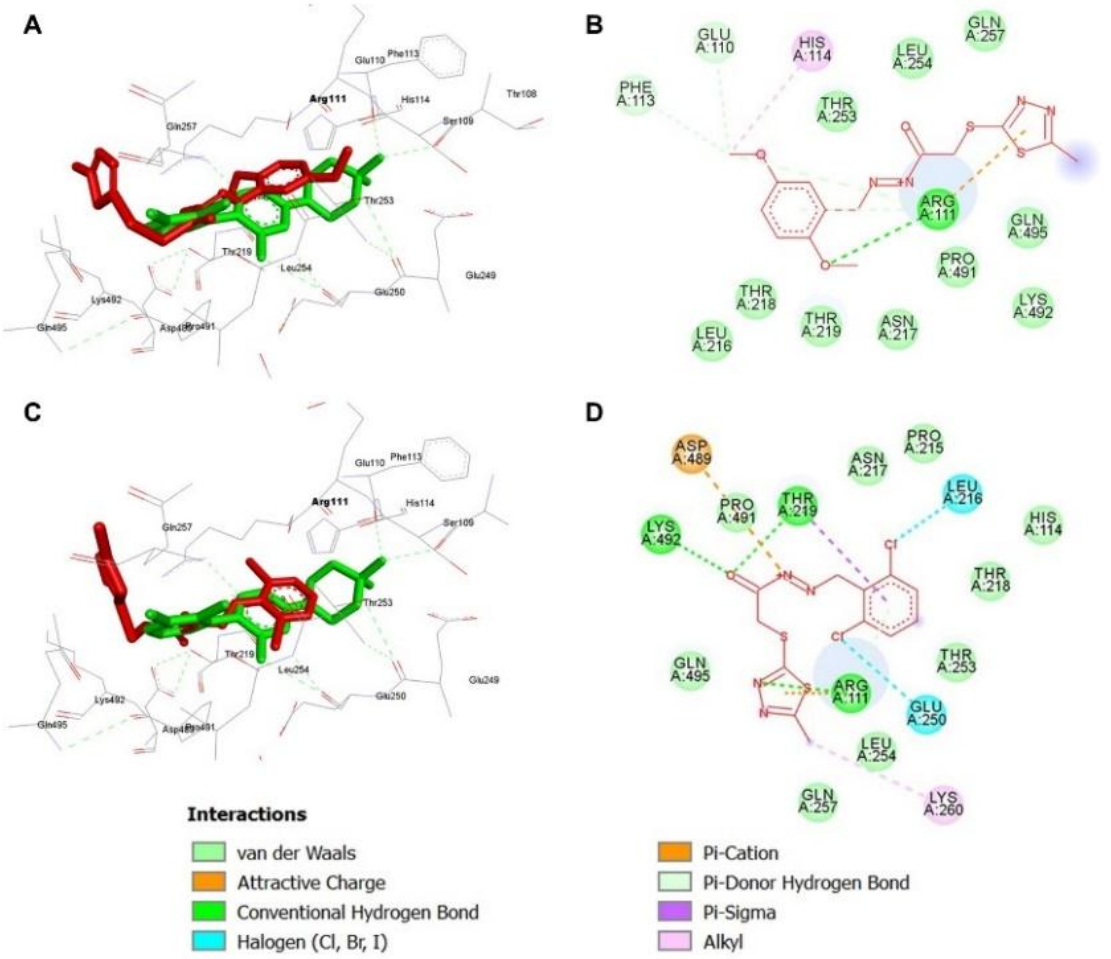

Figure 4.14. A) 3D orientation image of compound **TEH10** (red) with **SHP099** (green) in the tunnel allosteric site of 5EHR, B) 2D interaction map of compound **TEH10** (red) in the tunnel allosteric site of 5EHR; C) 3D orientation image of compound **TEH06** (red) with **SHP099** (green) in the tunnel allosteric site of 5EHR, D) 2D interaction map of compound **TEH06** (red) with **SHP099** (green) in the tunnel allosteric site of 5EHR.

B. Binding data of compound TEH06 within the crystal structure of 5EHR

Our *in vitro* enzymatic lead compound **TEH06** showed comparable affinity for SHP2 upon molecular docking. A detailed study of the 2D and 3D interaction pattern of the compound within the tunnel allosteric site of the enzyme (**Figure 4.14C** & **4.14D**) revealed a few salient features. Firstly, the ligand oriented itself within the binding site such that it showed appreciable overlap with the native ligand **SHP099**. As with compound **TEH10**, here too the substituted phenyl ring i.e., the 2,6-dichloro ring

showed a pi-pi type overlap with the central pyrimidine ring of **SHP099**. The thiadiazole part protrudes out of the binding cavity but shows stabilizing interactions with multiple amino acid residues like Arg111, Lys260, Gln495 etc. This is because the molecule takes on a curved configuration which makes the thiadiazole part accessible to Arg111 and other amino acid residues. The acyl hydrazone moiety also enters into multiple interactions with Thr219 (H-bonds), Asp489 (pi-cation bonds), Pro491 (van der Waals forces) and Lys492 (H-bonds). Multiple H-bonding interactions stabilize the molecule and lead to better affinity for the enzyme. Finally, the two chlorine atoms of the phenyl ring show halogen interactions with Leu216 and one of the members of the catalytic triad i.e., Glu250 thereby further activating the molecule for binding to SHP2.

4.3.3.2. Molecular dynamics simulation studies for compound TEH06

In order to evaluate the binding pattern of compound **TEH06** to the tunnel allosteric site of SHP2 enzyme (PDB ID: 5EHR) and to establish the effects of the interactions on the protein molecule structure, molecular dynamics simulation was performed on compound **TEH06** with the help of Desmond molecular dynamics software (Schrodinger Release 2021.1: Desmond Molecular Dynamics System, D. E. Shaw Research, New York, NY, 2021). The simulation was run for 100 ns at 300 K temperature and Maestro graphical user interface (Maestro, Schrodinger, LLC, New York, NY, 2021) was employed to analyse and visualize the outcomes. The various outcomes and visualizations of the MD run are collated in the simulation interactions diagram of compound **TEH06** with 5EHR (**Figure 4.15**).

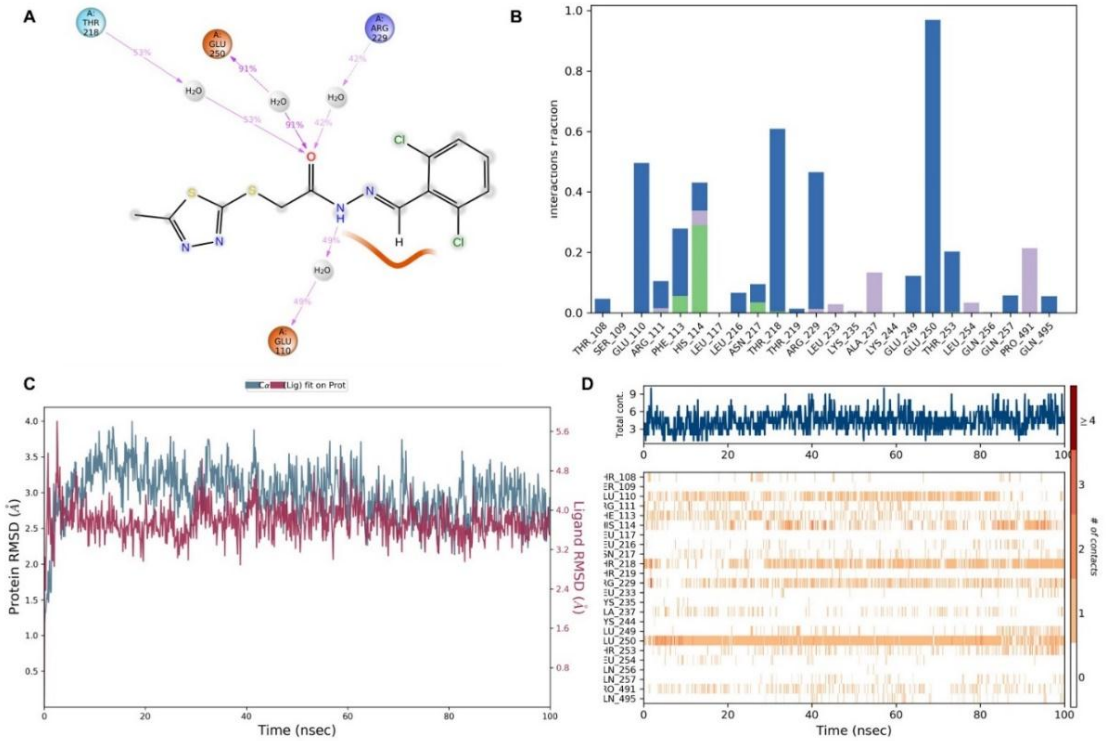

Figure 4.15. Protein-ligand contact diagrams ('simulation interactions diagrams') generated through Molecular Dynamics simulation of compound **TEH06** with SHP2 (PDB ID: 5EHR). A) Percent interaction of ligand with protein (represented by purple arrow). Red spheres represent electronegative species, blue spheres represent polar residues and solvent exposed areas are shown in grey. B) Stacked bar chart representing different types of protein-ligand contacts. Green histogram bars indicate hydrogen bond interactions; violet bars represent hydrophobic interactions whereas blue bars represent the water bridges between protein and ligand. C) Protein-ligand RMSD graph. Blue line represents apoprotein and red line represents ligand bound protein D) Protein-ligand contacts in timeline representation for 100 ns simulation; the top upper panel (blue) shows the number of contacts between protein and ligand throughout the simulation period and the bottom panel (orange) indicates the amino acid residues that interact with ligand at different time frame.

Figures 4.15A and **4.15B** show the various interaction types that the ligand undergoes with the protein where it can be seen that the atoms of the acyl hydrazone moiety are the primary ones that interact strongly. The protein and the ligand displayed different interactions throughout the course of the simulation viz. hydrogen bonds, hydrophobic interactions and water bridges. Water bridges were the predominant and some of the strongest interactions shown by the ligand with Glu250, Thr218, Arg229 and Glu110.

In fact, Glu250 which is part of the tunnel allosteric catalytic triad, interacted with the hydrazone carbonyl oxygen atom of the ligand for 91% of the total simulation period (**Figure 4.15A**). Phe113, another allosteric triad residue and the adjacent His114 showed H-bonding (green bar, **Figure 4.15B**). Analysis of the RMSD graph shown in **Figure 4.15C** tells us that association of SHP2 with compound **TEH06** does not cause any significant conformational changes to the protein. Also, the RMSD value changes fall within the acceptable range of 1-3 Å (on an average, the change observed here was of the order of 1.5-1.6 Å). Thus, it can be inferred from the MD simulation studies that compound **TEH06** showed conserved interactions like H-bonding and hydrophobic interactions with crucial amino acid residues of tunnel allosteric site of SHP2 and conferred better stability to the complex on binding with the enzyme.

4.3.3.3. Predicted ADMETox parameters

The predicted ADME and toxicological properties of compounds **TEH01** to **TEH21** are given in **Tables 4.7** and **4.8** respectively. All compounds displayed similar skin permeability with a value around -3.3 to -4. The blood-brain barrier (BBB) permeability ranges from 0.0717 for compound **TEH14** to 0.5662 for compound **TEH05**. The in vitro enzymatic lead molecule **TEH06** showed the second highest BBB permeability (0.4739) whereas the Caco2 and MDCK permeability were low to moderate. It bound to plasma proteins by up to 90.33% and was predicted to be an inhibitor of CYP2C9, CYP2C19 and CYP3A4. From the ADME data it can be assumed that all the molecules of this series are rather hydrophilic in nature and thus have better affinity for the polar amino acid residues lining most crucial parts of the enzyme. The toxicological data prediction also gave us an idea regarding the safety profile of the compounds. Expectedly enough, all compounds of this series were predicted to be mutagenic in

Ames test as these comprise of five-membered nitrogen-containing heterocycles which are known to be of mutagenic and genotoxic nature. Interestingly, all compounds showed negative carcinogenicity in mouse & rat model and about 50% of the molecules posed medium risk of hERG inhibition compared to the reference SHP2 inhibitors (**Table 4.8**). In sharp contrast, **SHP099** though being a mutagen in Ames test, showed positive carcinogenicity in mouse model and negative in rats. It can thus be inferred from the toxicological data that all compounds fall within a normal range of safety as sought for newly developed drugs.

Table 4.7. Predicted ADME properties of compounds **TEH01-TEH21, SHP099** and few clinical SHP2 inhibitors

Compd	MW	HIA (%)	Caco2	MDCK (nm/s)	SP (logKp, cm/h)	BBB	PPB (%)	CYP2C9	CYP2C19	CYP3A4
TEH01	292.38	94.95	3.9249	8.4938	-3.34	0.1715	79.65	inhibitor	inhibitor	inhibitor
TEH02	326.82	97.35	4.9315	2.7120	-3.41	0.3337	86.37	inhibitor	inhibitor	inhibitor
TEH03	326.82	97.35	24.0681	2.5009	-3.41	0.2827	87.37	inhibitor	inhibitor	inhibitor
TEH04	361.26	98.14	22.781	0.1885	-3.35	0.4310	90.05	inhibitor	inhibitor	inhibitor
TEH05	361.26	98.14	23.426	0.4012	-3.36	0.5662	89.42	inhibitor	inhibitor	inhibitor
TEH06	361.26	98.15	27.933	0.3510	-3.35	0.4739	90.33	inhibitor	inhibitor	inhibitor
TEH07	308.37	87.95	4.2463	4.4789	-4.28	0.1307	69.86	inhibitor	inhibitor	inhibitor
TEH08	308.37	87.95	6.088	7.5765	-4.26	0.1184	69.42	inhibitor	inhibitor	inhibitor
TEH09	322.40	93.64	5.2112	4.1589	-3.64	0.1288	74.89	inhibitor	inhibitor	inhibitor
TEH10	338.40	92.05	11.5532	6.5517	-3.83	0.1199	73.50	inhibitor	inhibitor	inhibitor
TEH11	382.45	90.17	11.2626	0.5444	-3.97	0.0898	74.41	inhibitor	inhibitor	inhibitor
TEH12	352.43	85.36	5.7407	1.9263	-4.22	0.1044	71.34	inhibitor	inhibitor	inhibitor
TEH13	337.37	72.90	0.7943	8.0596	-3.52	0.0749	78.17	noninhibitor	noninhibitor	noninhibitor
TEH14	293.36	90.24	5.3679	1.2054	-3.86	0.0717	54.92	inhibitor	inhibitor	inhibitor
TEH15	282.34	86.34	1.1001	5.8022	-3.65	0.1145	70.24	inhibitor	inhibitor	inhibitor
TEH16	306.40	95.60	4.387	6.3884	-3.37	0.1764	76.60	inhibitor	inhibitor	inhibitor
TEH17	324.39	95.65	3.754	5.4585	-3.68	0.2412	76.12	inhibitor	inhibitor	inhibitor
TEH18	340.84	97.63	6.290	1.9592	-3.44	0.3372	84.12	inhibitor	inhibitor	inhibitor
TEH19	385.30	98.12	19.294	0.2356	-3.31	0.3589	85.18	inhibitor	inhibitor	inhibitor
TEH20	322.40	89.28	4.283	2.8531	-4.23	0.1331	68.24	inhibitor	inhibitor	inhibitor
TEH21	351.40	75.72	0.706	4.2269	-3.50	0.0750	78.00	noninhibitor	noninhibitor	noninhibitor
SHP099	351.10	95.48	20.8851	0.1703	-3.03	0.0396	63.34	noninhibitor	noninhibitor	noninhibitor
BBP-398	377.27	93.01	19.5058	20.0513	-4.00	0.8690	72.90	inhibitor	noninhibitor	inhibitor
RMC-4630	450.45	93.44	18.1151	0.15284	-4.76	0.0485	42.30	inhibitor	noninhibitor	inhibitor
TNO155	421.96	91.73	16.7049	0.2355	-4.73	0.0525	65.82	inhibitor	noninhibitor	noninhibitor
JAB-3068	476.55	96.01	8.7239	0.1933	-4.24	0.0612	35.15	inhibitor	noninhibitor	noninhibitor
RLY-1671	454.53	93.18	18.7666	20.6928	-4.74	0.0490	61.09	inhibitor	noninhibitor	noninhibitor
HBI-2376	598.12	95.35	20.3995	0.1109	-4.77	0.0421	59.86	inhibitor	noninhibitor	inhibitor

HIA: Human Intestinal Absorption [0–20 (poor), 20–70 (moderate), 70–100 (well)], Caco2: In-vitro Caco2 cell permeability [<4 (low), 4–70 (moderate), >70 (high)], MDCK: Maden Darby Canine Kidney cell permeability [<25 (low), 25–500 (moderate), >500 (high)], SP: Skin permeability, BBB: Blood brain barrier permeability (C_{brain}/C_{blood}), PPB: In-vitro plasma protein binding.

Table 4.8. Predicted toxicological properties of compounds **TEH01-TEH21, SHP099** and few clinical SHP2 inhibitors

Compd	Ames test	Carcinogenicity (Mouse)	Carcinogenicity (Rat)	hERG inhibition
TEH01	mutagen	negative	negative	low risk
TEH02	mutagen	negative	negative	medium risk
TEH03	mutagen	negative	negative	medium risk
TEH04	mutagen	negative	negative	medium risk
TEH05	mutagen	negative	negative	medium risk
TEH06	mutagen	negative	negative	medium risk
TEH07	mutagen	negative	negative	medium risk
TEH08	mutagen	negative	negative	medium risk
TEH09	mutagen	negative	negative	medium risk
TEH10	mutagen	negative	negative	low risk
TEH11	mutagen	negative	negative	low risk
TEH12	mutagen	negative	negative	low risk
TEH13	mutagen	negative	negative	medium risk
TEH14	mutagen	negative	negative	medium risk
TEH15	mutagen	negative	positive	low risk
TEH16	mutagen	negative	negative	medium risk
TEH17	mutagen	negative	positive	medium risk
TEH18	mutagen	negative	negative	low risk
TEH19	mutagen	negative	positive	medium risk
TEH20	mutagen	negative	negative	low risk
TEH21	mutagen	negative	negative	low risk
SHP099	mutagen	positive	negative	medium risk
BBP-398	non-mutagen	positive	negative	medium risk
RMC-4630	non-mutagen	positive	negative	low risk
TNO155	mutagen	positive	negative	low risk
JAB-3068	non-mutagen	positive	negative	ambiguous
RLY-1671	non-mutagen	negative	negative	high risk
HBI-2376	non-mutagen	positive	negative	high risk

Ames test-Ames test for mutagenicity in *Salmonella typhimurium*, Carcinogenicity (Mouse)-2 years carcinogenicity bioassay in mouse, Carcinogenicity (Rat)-2 years carcinogenicity bioassay in rat, hERG inhibition-*In Vitro* Human Ether-a-go-go Related Gene Channel inhibition

For any molecule to become an effective drug, apart from its potency, it must reach to the site of action with sufficient concentration to produce the desired biological effect. In the BOILED-egg model [183], a plot of the computed (predicted) lipophilicity

(WLOGP) and polarity (total polar surface area, tPSA) of each molecule generates the boiled-egg construction where the yellow yolk represents lipophilic environment and mimics the blood-brain-barrier while the egg white represents hydrophilic environment and mimics the gastrointestinal tract. Thus, compounds that are predicted to have high probability of BBB penetration will fall in the yellow region while those having high probability of passive gastrointestinal absorption will be in the 'egg white' region. Yellow and white regions are not mutually exclusive. The blue point indicates that the molecule is expected to be the substrate of P-gp and will actively be effluxed by P-gp (PGP+) whereas red points indicate that molecule is not an expected substrate of P-gp (PGP-) and will not be actively effluxed from brain. For our compounds **TEH01-TEH21**, the above graph (**Figure 4.16B**) indicates that except five compounds, all the others will be absorbed from GIT but no compound is predicted to cross the BBB. This prediction is similar to that of the clinical SHP2 inhibitors (**Figure 4.16A**), though all our compounds are shown to be PGP negative. The BOILED-egg prediction is in corroboration with the ADME prediction of all our compounds.

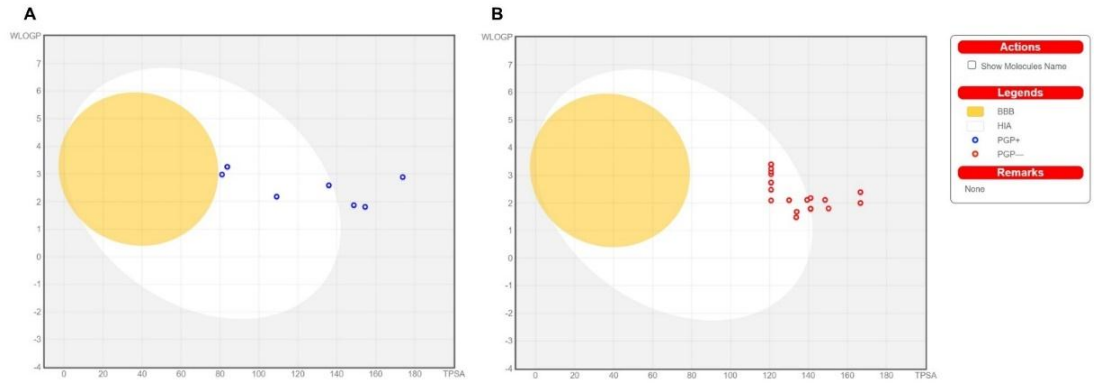

Figure 4.16. 'Brain Or IntestinaL EstimateD' permeation method **(**BOILED-egg) model based prediction of pharmacokinetic properties. A) BOILED-egg model of few clinical small molecule SHP2 inhibitors viz., **SHP099, BBP-398, RMC-4630, TNO155, JAB-3068, RLY-1671** and **HBI-2376**; B) BOILED-egg model of compounds **TEH01-TEH21**.

Few crucial PK and bioavailability parameters of the lead compound **TEH06** were predicted using Deep-PK, a robust machine learning method based on diverse molecular descriptors and graph neural networks developed by the Biosig Lab (The University of Queensland) to get a closer-to-reality idea about these 'end stage parameters' of our developed NCE. Parameters like steady-state volume of distribution (V_{Dss}), clearance (Cl), bioavailability (F%), drug half-life ($t_{1/2}$), maximum drug concentration (C_{max}) and time to reach C_{max} (T_{max}) were all calculated after a supposition of intravenous administration of the compound *t.i.d.* and are presented in **Table 4.9**. From the data, we can infer that compound **TEH06** is predicted to have favourable PK properties. With a predicted steady-state volume of distribution as high as 5.75 L/kg and a bioavailability of 74%, compound **TEH06** is presumably distributed homogenously across various tissues and would enter quite efficiently into the systemic circulation. A low $t_{1/2}$ indicates the compound will eliminate quickly from the body while T_{max} of 0.6 h is justifiable for i.v. administration and is within acceptable range for a desirable drug candidate.

Table 4.9. Predicted pharmacokinetic and bioavailability parameters of compound **TEH06**

Pharmacokinetic Parameter	Parameter Unit	Parameter Values
V_{Dss}	L/kg	5.75
Cl	(ml/min/kg)	5.16
F (Bioavailability)	%	74
$t_{1/2}$	h	1.78
C_{max} (free)	μM	5.74
T_{max}	h	0.6

V_{Dss}: steady-state volume of distribution, Cl: clearance, F: bioavailability, $t_{1/2}$: drug half-life, C_{max}: maximum drug concentration and T_{max}: time to reach C_{max}

4.4. Summary

Development of small molecule inhibitors of SHP2 is a valuable approach for the targeted therapy of various cancers due to the direct and multifaceted role of SHP2 in the progress of the disease. In our pursuit to develop novel and effective inhibitors of SHP2 for cancer therapy, we had previously identified and evaluated molecule **111675** as a moderately potent small-molecule SHP2 inhibitor through pharmacophore-based virtual screening followed by synthesis and biological evaluation *in vitro*. Improvement of this scaffold lead to development of a library of 21 *S*-acetohydrazones of 5-methyl-1,3,4-thiadiazole-2-thiol bearing a substituted benzylidene moiety (compounds **TEH01-TEH15** i.e., 15 compounds consisting of carbohydrazones of benzaldehyde derivatives and compounds **TEH16-TEH21**, i.e., 6 compounds consisting of carbohydrazones of acetophenone derivatives) through 'scaffold hopping' & lead simplification and were synthesized & characterized via spectroscopic techniques (**Figure 4.17**). The synthesized compounds were evaluated for their anti-SHP2 potential by an established *in vitro* enzyme inhibition assay using the DiFMUP-mediated fluorometric protocol wherein the molecules displayed micromolar to submicromolar activity against allosterically activated fl-SHP2 enzyme. Structure-activity correlations were made from the obtained enzymatic inhibition data. Subsequently, compound **TEH06** ((*E*)-*N*'-(2,6-dichlorobenzylidene)-2-((5-methyl-1,3,4-thiadiazol-2-yl)thio)acetohydrazide) emerged as the most potent SHP2 inhibitor (IC_{50} = 0.120 ± 0.006 μM). Its activity against SHP2 may be attributed to the presence of the privileged thioacetohydrazone linker coupled with the 2,6-dichlorophenyl ring in its structure which impart an optimum electronegativity and enhanced lipophilicity to the molecule.

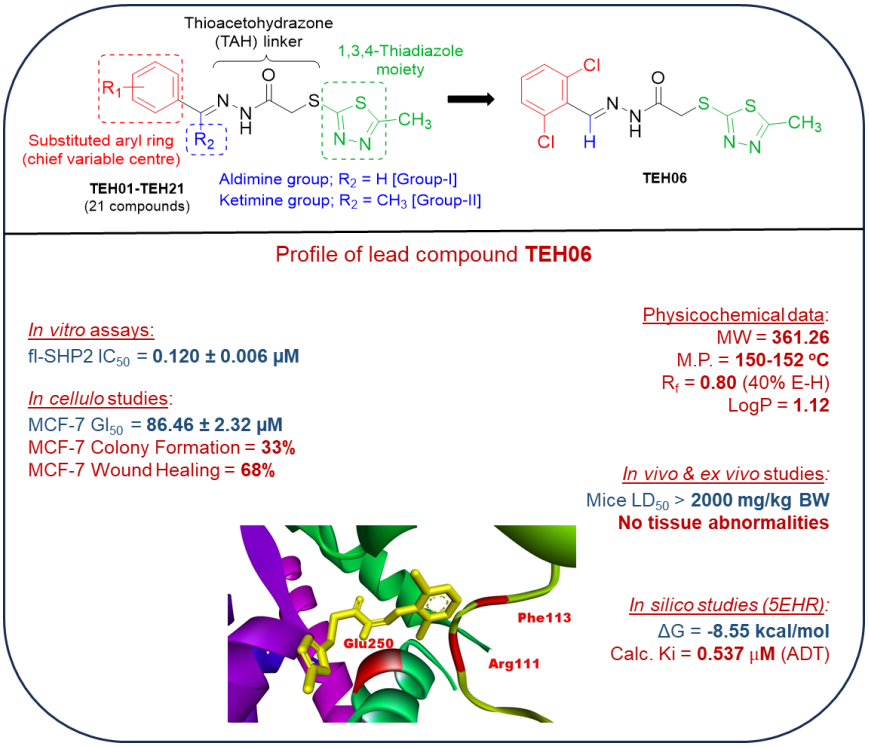

Figure 4.17. Summary of all findings for the current series **TEH01-TEH21**

In silico evaluation of the designed scaffold and the resultant library of compounds gave us an idea regarding the affinity of this series towards the tunnel allosteric site of SHP2 (PDB ID: 5EHR). Post-screening molecular docking of compounds **TEH01-TEH21** and pose analysis showed multiple interactions with Arg111 and Phe113 of 5EHR. The *in vitro* enzymatic lead compound **TEH06** showed multiple interactions with the key residues of the allosteric site, which corroborated its better binding affinity for SHP2 (ΔG = -8.55 kcal/mol) and it's *in vitro* efficacy against the enzyme. MD simulation studies revealed stabilizing interactions between the ligand and the protein and proved that compound **TEH06** occupies the tunnel allosteric site of SHP2.

Further, cell-based studies revealed compound **TEH06** to have moderate yet best-in-library cytotoxicity against human breast cancer cell line (MCF-7; IC_{50} = 86.46 ± 2.32 µM). Compound **TEH06** also exhibited moderate *in cellulo* anti-survival (33% colony formation) and anti-migratory effect (45% wound closure) on MCF-7 cells upon

treatment with sub-IC_{50} dose (5 μM) via a colony formation and scratch wound healing assay. *In vivo* toxicological evaluation of compound **TEH06** revealed excellent safety profile in mice as seen by an acute oral toxicity study at a high dose of 2000 mg/kg, where no animal was observed to be dead or in moribund state at the end of the experiment, their vital signs and organs were normal and the neurobehavioral, biochemical and haematological parameters did not show any signs of toxicity, whatsoever. In summary, our current study yielded a thioacetohydrazone bearing 1,3,4-thiadiazole coreld designed through systematic optimization of preceding inhouse leads which displayed submicromolar SHP2 inhibitory activity. The lead molecule identified from *in vitro* studies (compound **TEH06**) was moderately effective against the proliferation, survival and migration of human breast cancer cells with an excellent *in vivo* safety profile.